

OPTICAL PROPERTIES OF ATHERMALLY AND
THERMALLY ANNEALED HAFNIUM OXIDE
THIN FILMS ON SILICON

THESIS

Presented to the Graduate Council of
Texas State University – San Marcos
in Partial Fulfillment of
the Requirements

For the Degree

Master of SCIENCE

By

Heather M. Cain, B.S.

San Marcos, Texas
December 2003

COPYRIGHT

by

Heather Marie Cain

2003

ACKNOWLEDGEMENTS

I would like to thank Sematech for preparing the wafers, Naval Research Labs for laser shock-annealing the wafers, and Texas State University for supporting me financially during my research and writing of this thesis.

I would also like to thank my advisor, Dr. Donnelly, and the other members of my committee, Dr. Geerts and Dr. Gutierrez, for taking time to show me how to use the equipment and answering my questions.

Finally, I give sincere thanks to Dr. Crawford and Ms. Parks. If it weren't for them, I wouldn't even be here now.

This manuscript was submitted on November 12, 2003.

TABLE OF CONTENTS

	Page
LIST OF FIGURES	vi
Chapter	
I. INTRODUCTION	1
II. THEORY	3
Semiconductors	
MOSFET Technology	
Theory of FTIR	
Theory of Ellipsometry	
Capacitance-Voltage Analysis	
III. PROCEDURE	24
Annealing the Samples	
Measuring the Samples	
Determining Optical Constants	
IV. RESULTS AND DISCUSSION	28
Before Annealing	
Thermally Annealed Samples	
Athermally Annealed Samples	
V. CONCLUSIONS	40
APPENDICES	42
REFERENCES	58

LIST OF FIGURES

	Page
2.1 Band Structure	4
2.2 Silicon Lattice	6
2.3 MOSFET	6
2.4 Laser Shock Annealing	8
2.5 Michelson Interferometer	10
2.6 Electric Vectors at Interface	12
2.7 Parallel and Perpendicular Components of Electric Field	15
2.8 Null Ellipsometer	16
2.9 Mercury Probe	19
2.10 PNP Capacitor	19
2.11 Accumulation	20
2.12 Depletion	20
2.13 Inversion	21
2.14 C-V Curves	22
4.1 Absorbance of Silicon and Sample 6 Before Annealing	28
4.2 C-V Plot of HfO ₂ Before Annealing	30
4.3 Absorbance of Sample 6, Thermally Annealed	31
4.4 Peak Areas of Sample 6, Thermally Annealed	31
4.5 Calculated SiO ₂ Thickness of Sample 6 as a Function of Annealing Time. .	32
4.6 Index of Refraction of Sample 6, Thermally Annealed	33
4.7 C-V Curve of Sample 6, after 3 Minute Anneal	34

	Page
4.8 C-V Curve of Sample 6, after 35 Minute Anneal	34
4.9 Oxide Thickness of Sample 6, Thermally Annealed	35
4.10 Doping Concentration of Sample 6, Thermally Annealed	35
4.11 Reflectance of HfO ₂ , Athermally Annealed	36
4.12 Absorbance of Sample 1, Athermally Annealed	37
4.13 Absorbance Spectra of Sample 1, Athermally Annealed	37
4.14 Index of Refraction of HfO ₂ for Samples 1,2, and 3.	38
4.15 C-V Plot of HfO ₂ , Athermally Annealed	39

Chapter 1

INTRODUCTION

As semiconductors continue to decrease in size, the need to replace silicon dioxide (SiO_2) as the gate dielectric material becomes apparent. The International Technology Roadmap to Semiconductors¹ predicts the need for an oxide thickness of ≤ 1.3 nm for 2005. SiO_2 begins having problems with leakage current around 2.5 nm, due to carrier direct tunneling.² The minimum oxide thickness required to keep tunneling current from affecting device operation is 2 nm.³ Several materials with high dielectric constants are being studied as replacements for SiO_2 . A high dielectric constant is desirable because the dielectric constant is inversely proportional to the equivalent oxide thickness. A few candidates are HfO_2 , ZrO_2 , Ta_2O_5 , TiO_2 , and Si_3N_4 .³ HfO_2 is one of the most promising, being stable in direct contact with silicon and having a dielectric constant of ~ 28 -30, much higher than the dielectric constant of 3.9 for silicon dioxide.

Upon thermal annealing at temperatures above 600°C , a thin SiO_2 layer forms at the HfO_2/Si interface.³ Although the dielectric constant of the layer is ~ 9 - 10^3 and it is usually no more than a few nanometers thick, it causes the equivalent oxide thickness to increase. Another drawback of thermally annealing HfO_2 is that at 700°C , it crystallizes, causing leakage current along the grain boundaries.³ An alternative method to anneal the oxide without any thermal effects is to shock it with a high-intensity laser. This

technique has proved successful in annealing boron-doped silicon⁴, where the concentration of activated charge carriers was comparable to that in a thermally annealed sample. In addition, there was much less boron diffusion than in the thermally annealed sample.

The effects of athermal annealing on an oxide layer have not been studied yet. This research attempted to characterize some of the optical constants of athermally annealed HfO₂ and compare them to those of thermally annealed HfO₂.

It was found that the athermally annealed sample did not form a SiO₂ layer at the oxide/substrate interface, but the thermally annealed sample did. The index of refraction increased when annealed for the athermally annealed sample, and the equivalent oxide thickness decreased.

Chapter 2

THEORY

2.1 Semiconductors

All crystalline materials contain electrons that form what are called energy bands. The highest completely or partially filled non-conducting energy band is called the valence band. The next energy level up, which is empty at low temperatures in semiconductors, is called the conduction band. The energy separating the valence band from the conduction band is called the band gap. The band gap is a forbidden region where no stationary electron states can exist. Electrons can be excited from the valence band to the conduction band by thermal energy. Once there, the material becomes conducting.

Materials can be classified according to their band structure (Fig. 2.1⁵). In insulators, the valence band is completely filled, and no electrons can be moved by an electric field. Insulators also have large bandgaps, on the order of several eV, making it difficult for electrons to jump from the valence band to the conduction band. Metals have partially filled valence bands and negative bandgaps. This means that the bands overlap and the electrons are easily excited to the conduction band.

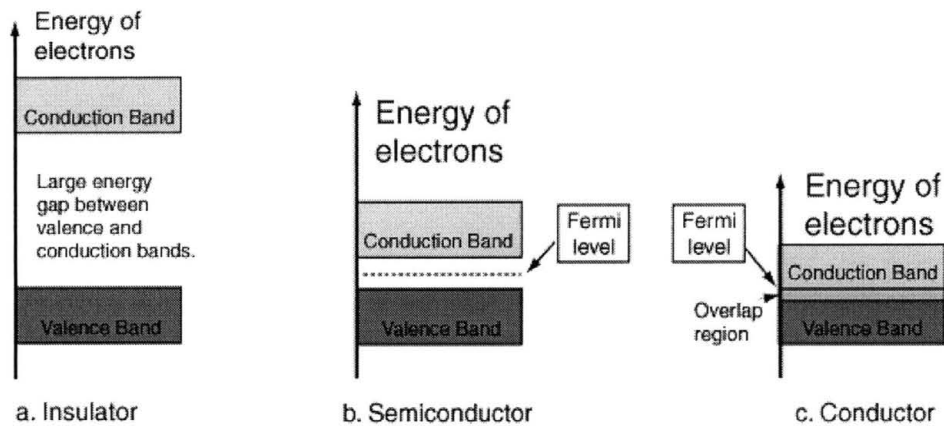


Figure 2.1⁵ Band Structure

Semiconductors have completely filled valence bands at low temperatures, but small bandgaps, usually from 0-2 eV. At high temperatures, the electrons are excited enough to jump from the valence band to the conduction band, and the semiconductor becomes conducting.

Intrinsic semiconductors, such as silicon, begin conducting at high temperatures when the electrons become excited. When an electron jumps to the conduction band, the valence band contains one less electron. The spot where the electron used to be is called a hole, and the hole can aid in conduction because electrons can jump into and out of it.

In intrinsic semiconductors, the number of electrons and holes is equal, and the concentration of each is $1.5 \times 10^{10} \text{ cm}^{-3}$ for silicon at room temperature. When a voltage is applied, the resistance is so great that the device overheats. More charge carriers need to be introduced to create a larger charge imbalance so that more current will flow when a voltage is applied. Semiconductors that have extra charge carriers are called extrinsic semiconductors.

The extra electrons or holes in extrinsic semiconductors come from doping, or adding impurities to the material. The dopants are elements from groups III or V. For example, suppose Si is the semiconductor material. Each atom contains four valence electrons that form bonds with the other Si atoms. If some of the Si atoms are replaced with phosphorus atoms (group V), four of the electrons from the phosphorus atom will bond with Si atoms, but there will be one extra electron. When an electric field is applied, the extra electron moves about the crystal and becomes a conduction electron. Such a device is called an n-type semiconductor.

Similarly, if an element from group III, such as boron, is added to the crystal, there will be a shortage of one electron. The missing electron, or hole, becomes conducting with an applied electric field, and the device is called a p-type semiconductor.

Impurities can be added to a semiconductor crystal by means of ion implantation. In this process, the semiconductor is placed in a vacuum and is bombarded with high-energy ions. The ions penetrate the crystal, colliding with atoms. When impurities are added to a crystal in this way, the lattice structure is often destroyed by the ion impact, causing the crystal to become amorphous and non-conducting. The lattice can be repaired and the impurity ions activated by annealing, or heating the wafer. Normally, the wafer is heated for 30 minutes between 800 and 1000°C.⁶ The high temperature allows the substrate atoms and the impurity atoms to move into their proper lattice sites, as in Fig 2.2⁷.

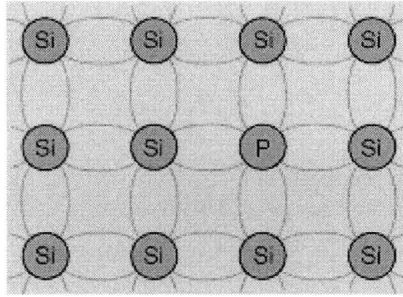


Figure 2.2 Silicon Lattice⁷

2.2 MOSFET Technology

Metal-oxide-semiconductor field-effect-transistor (MOSFET) devices are composed of a semiconductor substrate (usually silicon), an insulating oxide layer, and metal contacts (Fig. 2.3⁵). The substrate is usually p-type, and is doped with boron or aluminum. Two n-type regions are formed by ion implantation and are called the source and the drain. An oxide layer, called the gate oxide, is deposited on top of the substrate to serve as an insulator, and metal contacts on top of it allow current flow only between the source and drain.

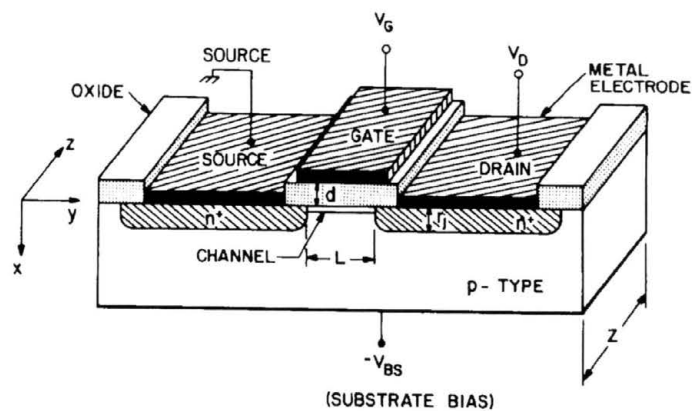


Figure 2.3 MOSFET⁵

Currently, the most common oxide used for gate dielectrics is silicon dioxide, SiO₂. It is easily grown by simply exposing the silicon substrate to oxygen at a high temperature. However, at thicknesses less than 2.5 nm, SiO₂ is no longer a good insulator.² Carrier direct tunneling allows electrons to tunnel through the oxide layer. The demand for smaller device sizes is rapidly increasing, and an oxide layer thinner than 2.5 nm is necessary. The easiest solution is to replace SiO₂ as the gate dielectric with a material that has a larger dielectric constant.

The equivalent oxide thickness is the thickness of the oxide in reference to a SiO₂ thickness. It can be calculated from the equation

$$EOT = d_{HfO_2} \frac{\epsilon_{SiO_2}}{\epsilon_{HfO_2}}, \quad (2.1)$$

where d_{HfO_2} is the thickness of the HfO₂ and ϵ_{SiO_2} is the dielectric constant of SiO₂, 3.9. Thus, an oxide with a dielectric constant larger than 3.9 can give an equivalent oxide thickness much less than the thickness of SiO₂ would be.

Some materials with high dielectric constants that are candidates for the gate dielectric are HfO₂, ZrO₂, Ta₂O₅, TiO₂, and Si₃N₄. Although all of these are promising, this research focuses on HfO₂ as the gate dielectric. The dielectric constant of HfO₂ is much higher than that of SiO₂ and ranges from 28-30.³

The oxide is usually deposited on the substrate before the annealing process. Unfortunately, the high temperature required for annealing the substrate also causes the atoms in the oxide layer to form a crystal lattice. When the oxide crystallizes, the grain boundaries serve as leakage current paths, and it is no longer a good insulator. HfO₂ crystallizes at 700 °C, but the silicon needs to be heated to at least 800 °C to anneal properly.³ In addition, at temperatures above 600 °C, silicon atoms drift into the oxide

layer and form an interfacial SiO₂ layer.³ This leads to a larger equivalent oxide thickness described by the equation

$$EOT = d_{SiO_2} + d_{HfO_2} \frac{\epsilon_{SiO_2}}{\epsilon_{HfO_2}}, \quad (2.2)$$

where d_{SiO_2} is the thickness of the SiO₂ layer.

In order for the HfO₂ to remain amorphous, the silicon needs to be annealed without using heat, or athermally annealed. This is possible with a new method called laser shock annealing. In this method, the sample is hit with a short, intense laser beam. The acoustical stress and shock waves spread outward, causing the silicon to anneal (Fig. 2.4).⁸

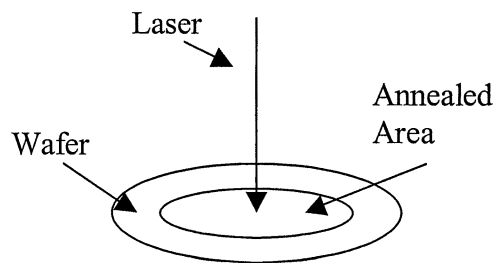


Figure 2.4 Laser Shock-Annealing

The effectiveness of athermal annealing on silicon has already been shown.⁸ This group showed that boron-doped silicon irradiated by a 5ns, 10 J laser pulse was annealed to a radius of ~1 cm away from the laser spot. High temperatures (>900 C) only exist within the ~1 mm spot; therefore, areas far from the center could not have been annealed by heat.

The area outside the crater is believed to have been annealed by mechanical energy. When a high-intensity laser hits the sample, all of the laser energy is absorbed by a plasma on the sample's surface. The hot plasma expands rapidly, creating shock waves that travel into the sample. At a depth of ~0.5 mm, the intensity of the shock waves decreases drastically, and the energy is transferred to mechanical waves within the sample that cause it to anneal.⁸

Until now, the effects of athermal annealing on an oxide layer have not been studied. It is expected that the absence of heat will prevent the oxide from crystallizing, but the mechanical energy will be enough to repair damage to the silicon and activate the donors.

2.3 Theory of FTIR

Fourier Transform Infrared Spectroscopy (FTIR) is a method used to gather reflectance and transmittance spectra of thin films. The simplest model of a spectrometer is the Michelson interferometer, developed in 1880 by Michelson and Morley.^{9,10} A diagram is shown in Figure 2.5.

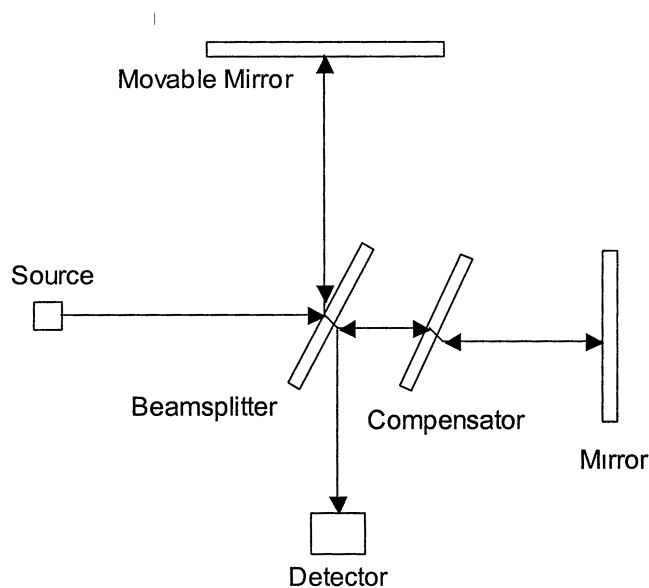


Figure 2.5: Michelson Interferometer

In the Michelson interferometer, light from the source is collimated by a mirror or lens. It then hits a beamsplitter and is divided into two beams of equal amplitude that go in different directions. One beam passes through a compensator plate to a fixed mirror, while the other beam strikes a movable mirror. Both beams are reflected back along the same path, where they hit the beamsplitter again, split again, and are partially recombined. Since the two beams traveled different path lengths, depending on the position of the movable mirror, they will interfere with each other.

The plot of intensity of the detected signal versus path difference is called an interferogram. The intensity of the interferogram is given by the equation

$$I_0(x) = B(\sigma_0)[1 + \cos(2\pi\sigma_0x)] \quad , \quad (2.3)$$

where $B(\sigma_0)$ is the detected signal, σ_0 is the wavenumber, and x is the path difference.

If a range of frequencies for the source is used, a superposition of the intensities of each wavelength pattern produces the interferogram, given by the equation

$$I_0(x) = \int_0^{\infty} B(\sigma)[1 + \cos(2\pi\sigma x)]d\sigma. \quad (2.4)$$

Fourier analysis of the interferogram will determine the intensity at each wavelength, and is usually plotted as intensity versus wavenumber. The inverse Fourier transform is

$$B(\sigma) = \int_0^{\infty} I(x) \cos(2\pi\sigma x)dx. \quad (2.5)$$

In FTIR, the infrared beam either passes through the sample or is reflected off it before reaching the detector. Measurements are taken with and without the sample. The spectrum without the sample is called the reference spectrum, and it contains features due to the beamsplitter and detector. The sample spectrum is divided by the reference spectrum to get rid of these instrumental effects. The resulting plot of intensity versus wavenumber is known as the transmittance spectrum if the beam passes through the sample, or the reflectance spectrum if the beam is reflected off the sample.

Fourier transform infrared spectroscopy can be used to determine the optical constants of thin films. Thickness, index of refraction, extinction coefficient, and dielectric constant can be found from reflectance or transmittance measurements. Transmittance measurements can only be used if the film is deposited on a transparent substrate. Since reflectance measurements can be used for transparent as well as opaque substrates, it is more common to use them.

One technique used to calculate optical constants from reflectance data is to fit the measured reflectance to a calculated reflectance $R(\lambda, n_1, k_1, d)$.⁹ $R(\lambda, n_1, k_1, d)$ is a function of three unknowns, index of refraction (n_1), extinction coefficient (k_1), and thickness (d), of the film at each wavelength.

The equation for reflectance is derived from the equations for an electromagnetic field at a boundary (Fig. 2.6¹¹).

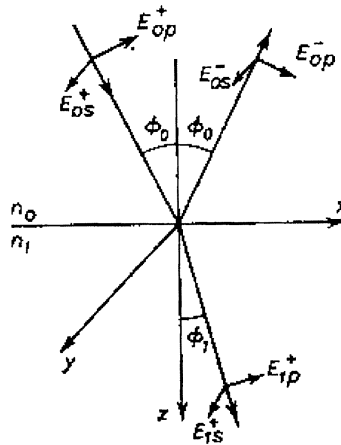


Figure 2.6¹¹ Electric Vectors at Interface

At the boundary, the equations for the electric and magnetic vectors in the x and y directions for the first medium (HfO_2) are

$$\begin{aligned}
 E_{0x} &= (E_{0p}^+ + E_{0p}^-) \cos \varphi_0 \\
 E_{0y} &= E_{0s}^+ + E_{0s}^- \\
 H_{0x} &= n_0 (-E_{0s}^+ + E_{0s}^-) \cos \varphi_0 \\
 H_{0y} &= n_0 (E_{0p}^+ - E_{0p}^-)
 \end{aligned} \tag{2.6}$$

and for the second medium (Si) are

$$\begin{aligned}
 E_{1x} &= E_{1p}^+ \cos \varphi_1 \\
 E_{1y} &= E_{1s}^+ \\
 H_{1x} &= -n_1 E_{1s}^+ \cos \varphi_1 \\
 H_{1y} &= n_1 E_{1p}^+
 \end{aligned} \tag{2.7}$$

After applying boundary conditions, we obtain the equations

$$\frac{E_{0p}^-}{E_{0p}^+} = \frac{n_0 \cos \varphi_1 - n_1 \cos \varphi_0}{n_0 \cos \varphi_1 + n_1 \cos \varphi_0} = r_{1p} \quad (2.8)$$

$$\frac{E_{0s}^-}{E_{0s}^+} = \frac{n_0 \cos \varphi_0 - n_1 \cos \varphi_1}{n_0 \cos \varphi_0 + n_1 \cos \varphi_1} = r_{1s}$$

If we assume normal incidence, these equations are equal and are

$$r_1 = \frac{n_0 - n_1}{n_0 + n_1} \quad (2.9)$$

for the air-oxide interface and

$$r_2 = \frac{n_1 - n_2}{n_1 + n_2} \quad (2.10)$$

for the oxide-substrate interface. r_1 and r_2 are called the Fresnel reflection coefficients.

Reflectance is the ratio of reflected energy to incident energy, and is given by

$$R = \frac{r_1^2 + 2r_1r_2 \cos 2\delta_1 + r_2^2}{1 + 2r_1r_2 \cos 2\delta_1 + r_1^2r_2^2}. \quad (2.11)$$

After substituting for r_1 and r_2 , the reflectance equation becomes

$$R = \frac{\left(\frac{n_0 - n_1}{n_0 + n_1}\right)^2 + 2\left(\frac{n_0 - n_1}{n_0 + n_1}\right)\left(\frac{n_1 - n_2}{n_1 + n_2}\right)\cos(2\delta_1) + \left(\frac{n_1 - n_2}{n_1 + n_2}\right)^2}{1 + 2\left(\frac{n_0 - n_1}{n_0 + n_1}\right)\left(\frac{n_1 - n_2}{n_1 + n_2}\right)\cos(2\delta_1) + \left(\frac{n_0 - n_1}{n_0 + n_1}\right)^2\left(\frac{n_1 - n_2}{n_1 + n_2}\right)^2} \quad (2.12)$$

and reduces to

$$R = \frac{(n_0^2 + n_1^2)(n_1^2 + n_2^2) - 4n_0n_1n_2 + (n_0^2 - n_1^2)(n_1^2 - n_2^2)\cos 2\delta_1}{(n_0^2 + n_1^2)(n_1^2 + n_2^2) + 4n_0n_1n_2 + (n_0^2 - n_1^2)(n_1^2 - n_2^2)\cos 2\delta_1} \quad (2.13)$$

where $\delta_1 = \frac{2\pi}{\lambda}n_1d_1$ for normal incidence.

If we set this reflectance equation equal to a fit on our experimental data, we should be able to determine the constants n_0 , n_1 , and n_2 . For absorbing films, we would have to

use the complex $n=n-ik$, where k is the extinction coefficient. For non-absorbing films, the extinction coefficient is zero. Since hafnium oxide is a dielectric and non-absorbing, k will always be zero, and we can simply use the real part of n .

The index of refraction n_0 refers to vacuum, n_1 is the oxide layer, and n_2 is the silicon substrate. The index of refraction of silicon is wavelength-dependent. At $\lambda=2000$ nm, silicon's $n=3.449$ and $k=0$. The index of refraction of a vacuum is 1 for all wavelengths. The index of refraction of HfO_2 , n_2 , is what needs to be determined.

FTIR can also be used to detect oxide formation by analyzing an absorbance spectrum. Absorbance can be derived from transmittance by the formula

$$\text{Absorbance} = \log \frac{100}{\% \text{Transmission}} \quad (2.14)$$

The optical phonon region of oxygen in the absorbance spectrum is between 1000-1300 cm^{-1} .¹² There is initially a peak centered at ~ 1100 cm^{-1} due to the silicon substrate. If the peak gets larger, that means there is formation of oxide, in this case either more HfO_2 or SiO_2 .

2.4 Theory of Ellipsometry

Light is composed of an electric field and a magnetic field that oscillate in a plane perpendicular to the direction of propagation. The polarization of light is described only by the electric field. An electric field oscillating in a direction parallel to the plane of incidence is labeled E_p , and one oscillating perpendicularly to the plane of incidence is labeled E_s (Fig. 2.7). Light that is composed of only one of these components is linearly polarized. Light that is made up of both components with equal magnitudes out of phase

by 90 degrees is circularly polarized. If both E_p and E_s are present but have different magnitudes, the light is elliptically polarized.

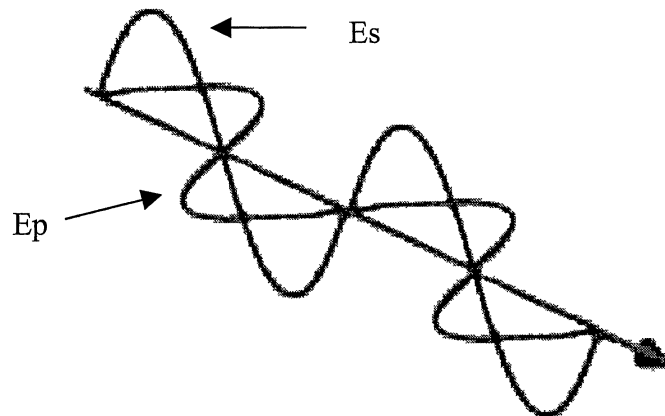


Figure 2.7 Parallel and Perpendicular Components of Electric Field

When light is reflected from a surface, its phase and amplitude change. The phase shift is caused by the surface itself, while the amplitude change, or attenuation, depends on the initial polarization of the light. For example, if the incident beam is linearly polarized, the reflected beam may become elliptically polarized. By measuring the phase shift and attenuation with an ellipsometer, information about the surface is revealed.

The Gaertner 117 Null Ellipsometer has a 632.8 nm HeNe light source. The light first passes through a polarizer to become linearly polarized. Then it passes through a quarter-wave plate that has been rotated 45 degrees out of the plane of incidence. It circularly polarizes the light by causing half of the electric fields to undergo a 90° phase shift. When light is reflected off the surface of the sample, the two components of the electric field again experience phase shifts and attenuation of different amounts.

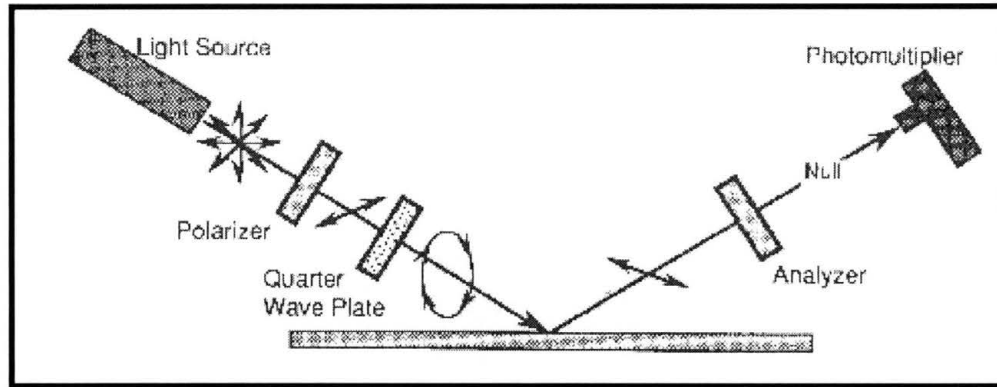


Figure 2.8¹³ Null Ellipsometer

Using the Fresnel reflection coefficients from equation 2.9, the total reflection coefficients of the parallel and perpendicular components of light for a single film are

$$R_p = \frac{r_{p12} + r_{p23}e^{-2i\beta}}{1 + r_{p12}r_{p23}e^{-2i\beta}} \quad (2.15a)$$

$$R_s = \frac{r_{s12} + r_{s23}e^{-2i\beta}}{1 + r_{s12}r_{s23}e^{-2i\beta}} \quad (2.15b)$$

The phase change, β , of the wave in the film is given by

$$\beta = 2\pi \left(\frac{d}{\lambda} \right) N_2 \cos \phi_2, \quad (2.16)$$

where N_2 is the complex index of refraction of the film, d is the film thickness, and ϕ_2 is the angle of the wave with respect to the normal inside the film. If multiple layers are present, equation 2.15 is first used to calculate the total reflection coefficients for the bottom layer. The coefficients for the next layer can then be calculated by inserting the first R into equations 2.15 as r_{23} .

The attenuation of the wave is described by the equation

$$\tan \Psi = \frac{|R_p|}{|R_s|} \quad (2.17)$$

and the phase shift is given by the equation

$$\Delta = \delta_p - \delta_s = \arg(R_p) - \arg(R_s), \quad (2.18)$$

where δ_p and δ_s are the phase shifts of the parallel and perpendicular light on reflection.¹³

The quantities Δ and Ψ are related to the total reflection coefficients (equation 2.15) by

$$\tan \Psi e^{i\Delta} = \frac{R_p}{R_s} \quad (2.19)$$

The light undergoes a phase shift when passing through the polarizer and quarter-wave plate. The polarizer is rotated until this first phase shift is opposite to the phase shift caused by reflection from the sample. This results in a net phase shift of zero and linearly polarized light. The reflected light then passes through an analyzer, which is rotated so as not to allow any of the linearly polarized light through, making the signal at the detector null. This technique is often referred to as null-ellipsometry.

The positions of the polarizer and analyzer can be used to determine information about the film. Measurements are always taken at two positions for each incident angle, since there are two positions of the polarizer and analyzer at which the detector signal will be null. The two polarizer positions are called P1 and P2, and the two analyzer positions are called A1 and A2. The attenuation, Ψ , is calculated from the equation

$$\Psi = \frac{180 - (A2 - A1)}{2} \quad (2.20)$$

The phase shift, Δ is calculated from the equation

$$\Delta = 360 - (P1 + P2) \quad (2.21)$$

Using equation 2.19, it is possible to calculate the thickness, index of refraction, and extinction coefficient of a transparent film from the measured Δ and Ψ . Each independent ellipsometric measurement will determine two unknown parameters. By

taking measurements at different angles of incidence, it is possible to determine more than two quantities from the ellipsometric data. In this research, the index of refraction and extinction coefficient for silicon are known. The extinction coefficient of HfO_2 is zero, since it is non-absorbing. The only unknowns are the index of refraction and thickness of the HfO_2 and SiO_2 layers. So measurements must be taken at two angles of incidence.

The values for Δ and Ψ at both angles can be entered into the FilmWizard program. This software will calculate thicknesses and indices of refraction using the Fresnel equations for reflection.¹³

2.5 Capacitance–Voltage Analysis

Capacitance-voltage analysis is performed using a mercury probe (Fig. 2.9¹⁴). It consists of a stainless steel contact held against the back of the sample. The front of the sample is under vacuum pressure to hold a mercury contact against it. The area of the mercury contact is $4.717 \times 10^{-3} \text{ cm}^2$.

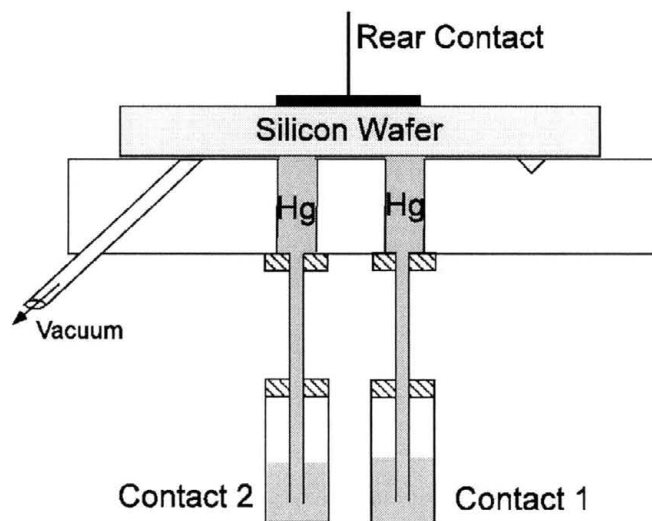


Figure 2.9¹⁴ Mercury Probe

Doping concentration and equivalent electrical thickness of the sample can be determined from capacitance-voltage (C-V) measurements. Leakage current can be determined from a current-voltage (I-V) curve.

The metal contact, oxide layer, and p-type silicon act like a metal-oxide-semiconductor (MOS) capacitor (Fig. 2.10¹⁵). In this figure, the semiconductor is p-type and N_A is the doping concentration of acceptors. If a voltage V is applied to the metal contact, the metal-oxide junction will be reverse biased and a depletion region will form.

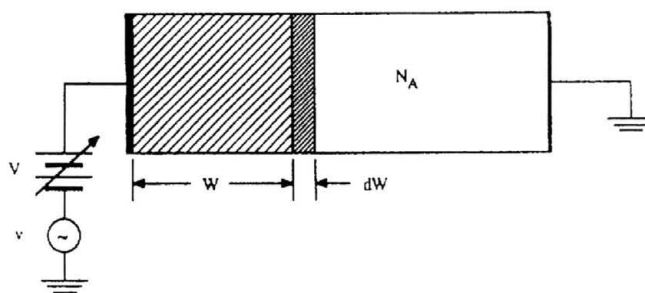


Figure 2.10¹⁵ PNP Capacitor

When a negative voltage is applied to a p-type semiconductor, positive charges within the semiconductor are attracted to the surface. This large number of majority carriers, or holes, near the surface is a condition called accumulation (Fig. 2.11). When a positive voltage is applied, the holes are pushed away from the surface, creating what is known as a depletion region (Fig. 2.12). As the positive applied voltage is increased the depletion region continues to widen until there are more electrons at the surface than holes. This condition is called inversion (Fig. 2.13). When the system is in inversion, the capacitance increases to a maximum.¹⁵

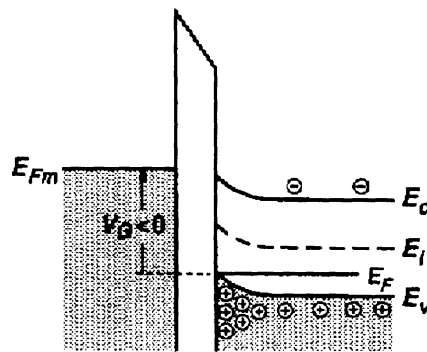


Figure 2.11¹⁶ Accumulation

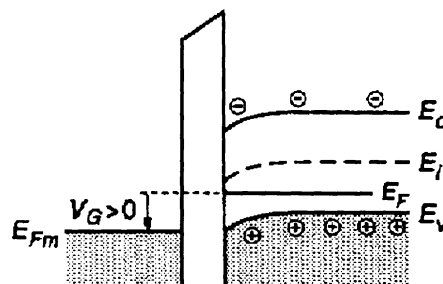
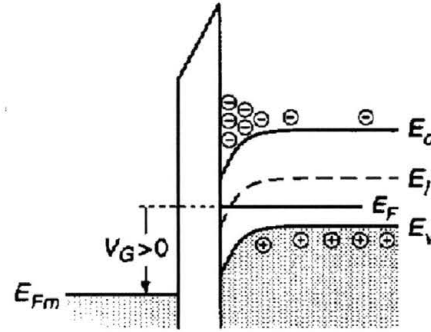


Figure 2.12¹⁶ Depletion

Figure 2.13¹⁶ Inversion

The width of the depletion region depends on the applied voltage, V , and can be calculated from a capacitance-voltage measurement. The capacitance is given by

$$C = -\frac{dQ}{dV}, \quad (2.22)$$

where Q is the charge of the semiconductor. A small ac voltage is applied to the metal contact to obtain the capacitance. The ac voltage creates a charge increment in the metal contact, which requires an equal and opposite charge increment in the semiconductor.

The semiconductor charge increment, dQ , is given by

$$dQ = -qAN_A(W)dW, \quad (2.23)$$

where A is the area of the metal contact and $N_A(W)$ is the concentration of charge carriers in the semiconductor at depth W . Plugging this into Eq. 2.22 gives

$$C = qAN_A(W)\frac{dW}{dV}. \quad (2.24)$$

If the capacitor is modeled as a parallel plate capacitor, the semiconductor capacitance is

$$C_s = \frac{K_s \epsilon_0 A}{W}, \quad (2.25)$$

where K_s is the dielectric constant of the semiconductor. If an oxide layer is present, the total capacitance is

$$C = \frac{C_{ox} C_s}{C_{ox} + C_s}, \quad (2.26)$$

where C_{ox} is the capacitance of the oxide. The thickness of the oxide layer is

$$W = K_s \epsilon_0 A \left[\frac{1}{C} - \frac{1}{C_{ox}} \right]. \quad (2.27)$$

Capacitance-voltage measurements can be taken at low-frequency or high-frequency dc and ac voltage sweeps. Figure 2.14 shows some ideal low-frequency (LF), high-frequency (HF), and deep depletion (DD) C-V curves. The low-frequency curve occurs when both the dc and ac voltage sweeps are slow enough to allow an inversion charge to form and respond to the ac frequency. The high-frequency curve occurs when the dc sweep is slow enough to allow an inversion charge to form, but the ac sweep is too fast for the inversion charge to be able to respond to it. The deep depletion curve occurs when the dc sweep is so fast the an inversion charge cannot even form.¹⁵

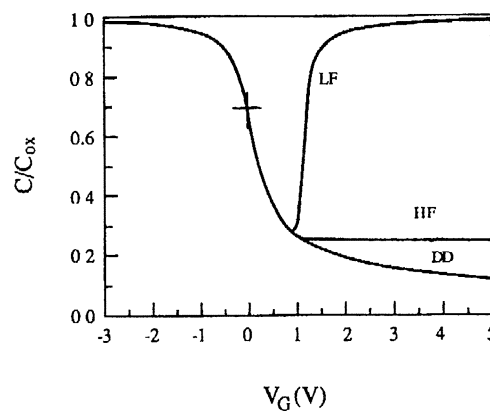


Figure 2.14¹⁵ C-V Curves

When the system is in strong inversion, as in the low-frequency case, the doping concentration can be found using the maximum-minimum capacitance technique. This

technique yields an average concentration over the entire depletion width. For a p-type MOS capacitor, the doping concentration can be calculated by measuring the maximum capacitance, C_{ox} , in strong accumulation and the minimum capacitance, C_{min} , in strong inversion. The equation to obtain the doping concentration for silicon at room temperature is

$$\log(N_A) = 30.38759 + 1.68278 \log\left(\frac{C_{sf}}{A}\right) - 0.03177 \left[\log\left(\frac{C_{sf}}{A}\right) \right]^2, \quad (2.28)$$

where $C_{sf} = \frac{RC_{ox}}{1-R}$ and $R = \frac{C_{min}}{C_{ox}}$. In this equation, C_{sf} is in farads, N_A is in cm^{-3} , and A is in cm^2 . The equation for an n-type MOS capacitor would be the same except N_D is used instead of N_A .¹⁵

Chapter 3

PROCEDURE

3.1 Annealing the Samples

Six samples of hafnium oxide on silicon were measured. The oxide layer was deposited onto the silicon by sputtering at International Sematech in Austin, TX. The samples measured approximately 3 cm^2 and the nominal thickness of the oxide was 50 nm.

Samples 1, 2, 3, and 4 were sent to the Naval Research Labs to be laser shock-annealed. A 30 ns laser pulse with intensity $10^{12} - 10^{13} \text{ W/cm}^2$ struck the sample, and it is believed that the acoustical shock waves caused the silicon to anneal. Samples 1, 2, and 3 were hit on the front side (oxide side), while sample 4 was hit on the backside (silicon side).

Samples 5 and 6 were thermally annealed in a Thermolyne tube furnace in a nitrogen ambient atmosphere. A bubbler was used to monitor the nitrogen flow. The samples were cooled at room temperature for at least five minutes before being measured. Sample 5 was heated continuously for one hour at $1000 \text{ }^\circ\text{C}$. Sample 6 was heated for periods of one minute at $950 \text{ }^\circ\text{C}$ for a total of 35 minutes. After each period of heating it was cooled and measured.

3.2 Measuring the Samples

Three types of measurements were made on the samples. These were reflectance and transmittance measurements by FTIR spectroscopy, ellipsometry, and capacitance-voltage. Samples 1, 2, 3, and 5 were measured before and after annealing. Sample 6 was measured before heating, and after each one-minute heating step, for a total of 35 measurements.

FTIR spectroscopy was performed using a Bomem DA3 Series Fourier Transform Spectrophotometer. At each location, both reflectance and transmittance measurements were taken. First, a reference spectrum was taken with no sample. The reference spectrum contains features due to the beamsplitter and detector. It was subtracted from the transmittance and reflectance spectra of the samples to reveal only those features due to the samples. An aperture size of 5 mm was used, and each measurement consisted of 300 scans. For samples 1, 2, and 3, measurements were taken at the crater center, 3 mm outside the crater center, and 1.3 cm outside the crater center.

Ellipsometry was performed with a Gaertner 117 Null Ellipsometer with a 632.8 nm HeNe laser. After the sample was cleaned and placed on the stage, the polarizer and the analyzer were rotated until a minimum reading was obtained on the extinction meter, indicating the light was linearly polarized. There are two possible positions in which linear polarization can be achieved, and the polarizer and analyzer readings were recorded for both of these. Then Δ and Ψ were calculated using equations 2.20 and 2.21.

At each position, a calibration reading was taken using a silicon sample of known thickness. The calibration data was used to find the exact angle of incidence. The Δ and

Ψ values were entered in the FilmWizard program to calculate thickness, index of refraction, and extinction coefficient of the oxide layer.

A Materials Development Corporation mercury probe was used to obtain capacitance-voltage data. The contacts have an area of $4.717 \times 10^{-3} \text{ cm}^2$. Measurements were taken with a Keithley 590 CV analyzer using a stimulus of 100 kHz, which yielded the desired low-frequency curve behavior. Also used were a step size of 0.1V through a range of -20 to $+20$ V and a time delay of 1s. Samples 2, 3, and 5 were too small to fit under the mercury probe contacts, so measurements were only made on samples 1 and 6.

3.3 Determining Optical Constants

The data from the above measurements was used to calculate the index of refraction, equivalent oxide thickness, and the doping concentration of the HfO_2 and SiO_2 layers.

The FilmWizard program was used to analyze the Δ and Ψ from the ellipsometry data. First a model of the materials was created, consisting of ambient atmosphere, SiO_2 , HfO_2 , and Si substrate. The optical data (index of refraction and extinction coefficient) for silicon and SiO_2 at 632.8 nm was loaded from the database, and the silicon thickness was assumed to be infinitely thick. The nominal thickness of 50 nm for the HfO_2 layer was used, along with an extinction coefficient of zero.

The exact angles of incidence were calculated from the calibration data, and the measurements taken at these angles were entered. Optimization was performed to find the index of refraction of HfO_2 and the thickness of the HfO_2 and SiO_2 layers.

The equivalent oxide thickness and doping concentration were found from the capacitance-voltage measurements. The oxide capacitance and minimum capacitance

were found from the C-V plot and used in equations 2.27 and 2.28. The oxide thickness found by equation 2.28 was used to calculate the equivalent oxide thickness (EOT), which is the thickness of the oxide relative to SiO₂. Equation 2.1 was used to calculate the EOT. The dielectric constant of SiO₂ is known and is 3.9. A dielectric constant of 28 was used for HfO₂.

The relation between the dielectric constant and the index of refraction is as follows:

$$n = \sqrt{\epsilon\mu} \quad (3.1)$$

where n is the index of refraction, ϵ is the dielectric constant, and μ is the relative permeability. At visible wavelengths, the relative permeability is ~ 1 for all materials.

The FTIR data was used to verify the presence of an oxide layer. First, the transmittance data was converted into absorbance data using the formula

$$Absorbance = \log \frac{100}{\%Transmission} \quad (3.2)$$

Then, the 1000-1300 cm⁻¹ region was analyzed. Peaks in this region correspond to optical phonon modes of SiO₂.¹² The area under the peaks for the thermally and athermally annealed samples was measured using Grams spectral analysis software.

An attempt also was made to determine the index of refraction of the oxide layers from the reflectance spectra. However, this method proved unsuccessful with the available software, mainly because an adequate fit for the curves could not be obtained.

Chapter 4

RESULTS AND DISCUSSION

4.1 Before Annealing

4.1.1 FTIR Results

Absorbance spectra of pure silicon and sample 6 before heating are shown in figure 4.1. Before annealing, the peak centered at 1107 cm^{-1} is due to oxygen in the silicon. After annealing, the area under this peak will increase due to oxide phonon absorbance. This peak will later be compared to the peaks of the annealed samples. An increase in peak size will indicate that more oxide phonons are being absorbed and that they must be coming from either an increase in the HfO_2 thickness or the formation of SiO_2 .

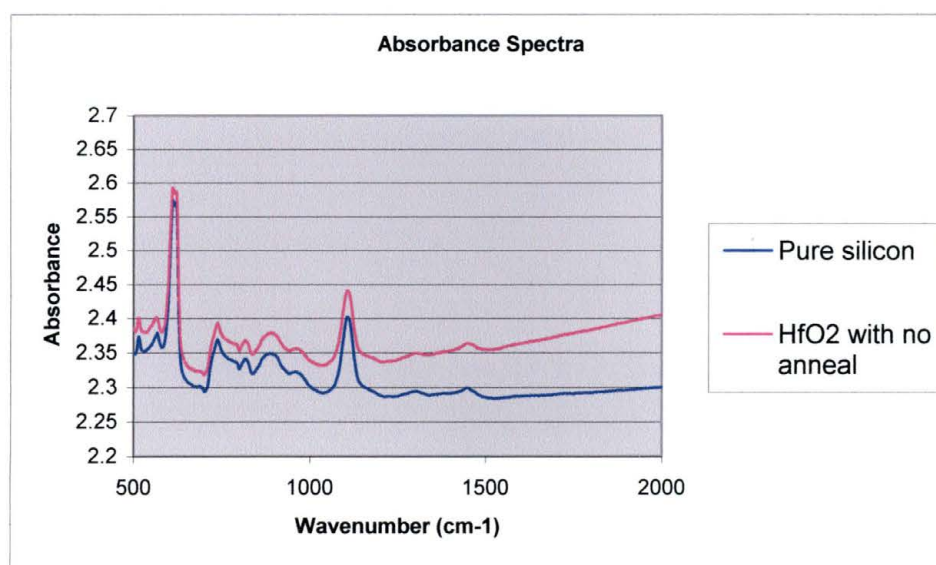


Figure 4.1 Absorbance of Silicon and Sample 6 Before Annealing

4.1.2 Ellipsometry Results

Sample 6 before annealing was found to have an index of refraction of 1.9796 at 632.8 nm and a thickness of 24.1927 nm. The accepted value for the index of refraction of HfO₂ at 632.8 nm is 1.9134. When a model of Si/SiO₂/HfO₂ was used with FilmWizard, the calculated thickness for SiO₂ was zero. From this it was determined that no interfacial layer of SiO₂ was initially present between the oxide and the substrate. The Δ and Ψ data for sample 6 are given in Appendix A.

4.1.3 C-V Analysis Results

The C-V curve for sample 6 before annealing is shown in figure 4.2. The oxide thickness calculated from the curve was 24.3 nm, only slightly different from the thickness calculated from the ellipsometry data. The average donor concentration (from equation 2.28) for sample 1 is $3.03 \times 10^{12} \text{ cm}^{-3}$. The system does not appear to go into inversion, probably due to the fact that the donors have not yet been activated by annealing.

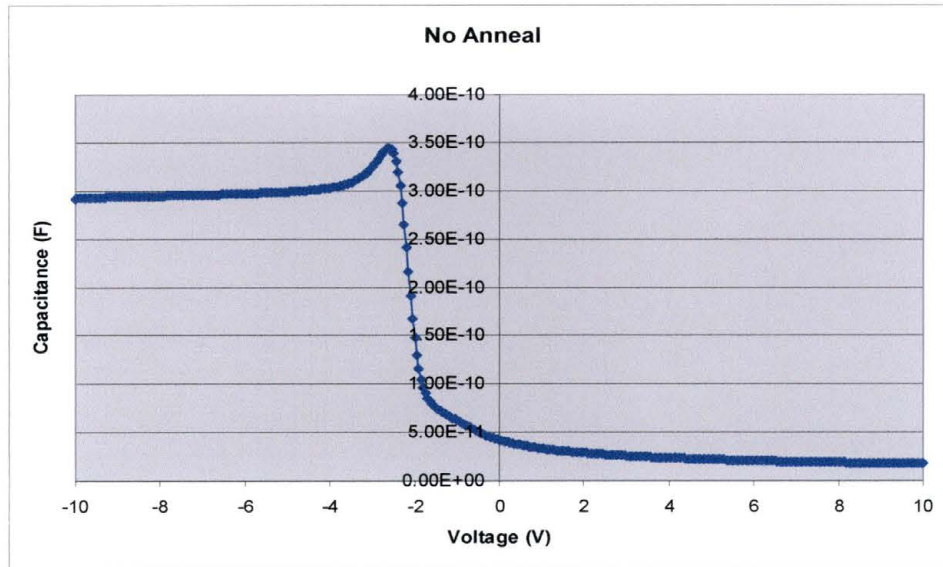


Figure 4.2 C-V Plot of HfO₂ Before Annealing

4.2 Thermally Annealed Samples

4.2.1 FTIR Results

The FTIR absorbance spectra of sample 6 indicate that the thickness of the oxide layer increased as the sample was heated. As seen in the absorbance spectra in figure 4.3, there is a peak around 1100cm^{-1} , in the oxide phonon absorbance region. The area under the peak increases with annealing time. Since the thickness of the HfO₂ layer was not increasing (see section 4.2.2), this can only indicate that the SiO₂ layer was growing.

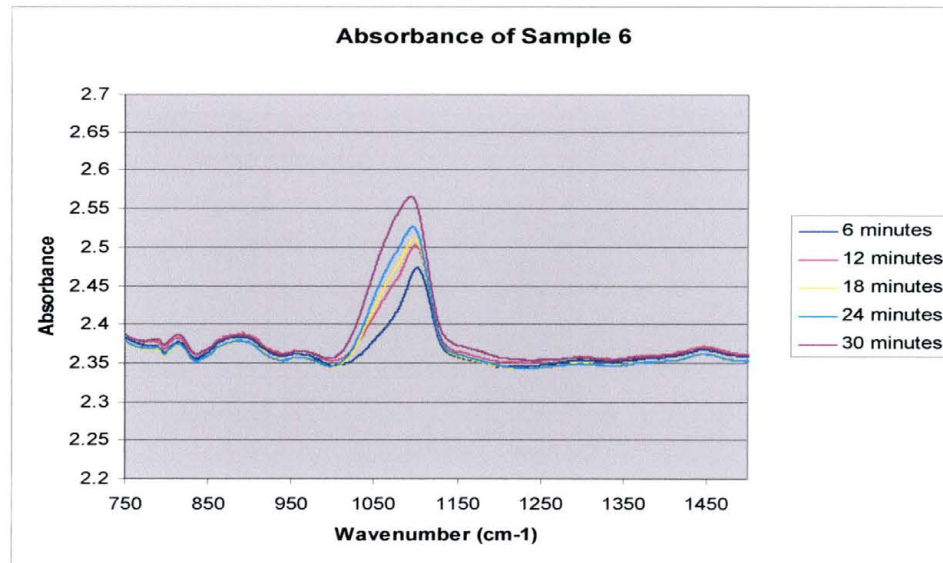


Figure 4.3 Absorbance of Sample 6, Thermally Annealed

Figure 4.4 shows a plot of the area under the curve increasing with time.

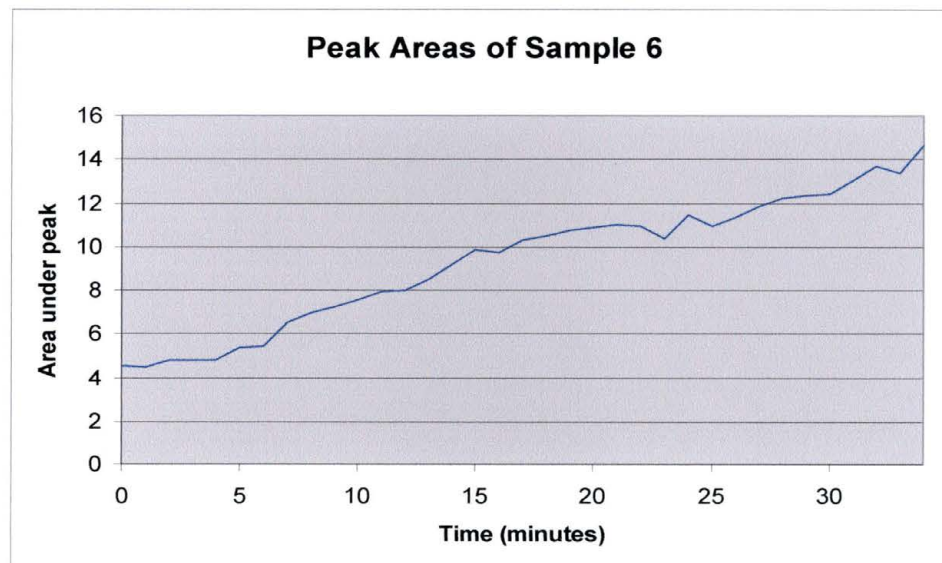


Figure 4.4 Peak Areas of Sample 6, Thermally Annealed

4.2.2 Ellipsometry Results

A layer of SiO_2 was found to form at the oxide/substrate interface of samples 5 and 6. The samples initially had no interfacial layer, but as the sample was heated, silicon diffused into the oxide layer and a SiO_2 layer formed. The SiO_2 layer on sample 5 after

heating for an hour was found to be 58.678 nm thick. On sample 6, the thickness of the SiO₂ layer increased to ~60 nm, as seen in Fig. 4.5, while the thickness of the HfO₂ layer remained constant at ~25 nm, as calculated from the ellipsometry data.

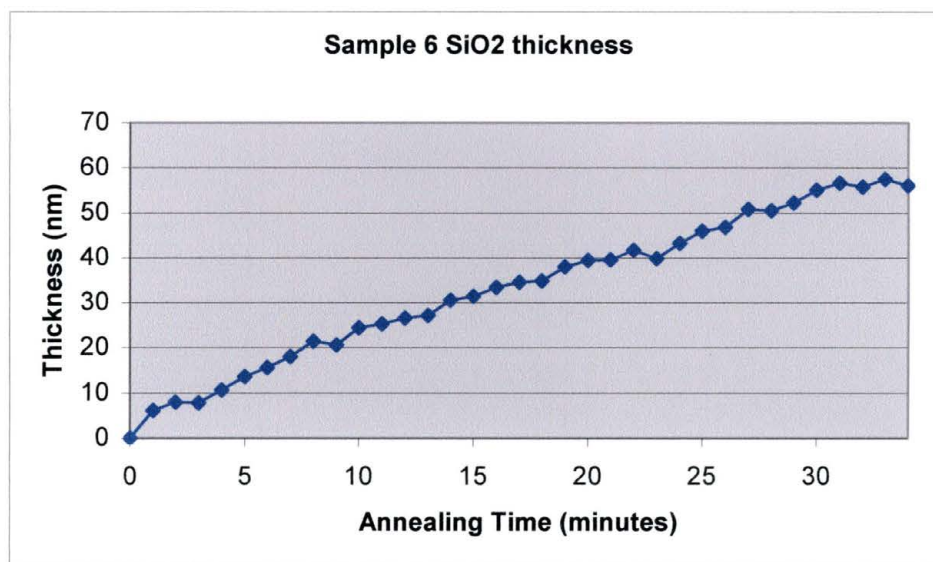


Figure 4.5 Calculated SiO₂ Thickness of Sample 6 as a Function of Annealing Time

For sample 5, the index of refraction after heating increased to 2.047. Before annealing, sample 6 had an index of refraction of 1.9796. During annealing, the index of refraction remained relatively constant, as seen in Fig. 4.6. The values toward the end of the chart are sporadic. By this time, the sample had been exposed to mercury over 30 times. Each time, the mercury would eat away a small amount of the film, so measurements taken in these spots may not be reliable.

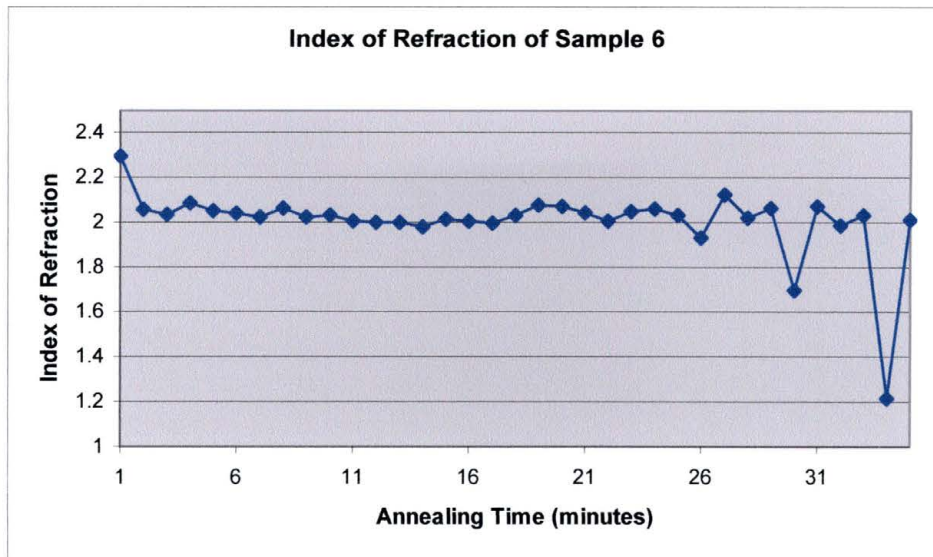


Figure 4.6 Index of Refraction of Sample 6, Thermally Annealed

4.2.3 C-V Analysis Results

C-V analysis could not be performed on sample 5 due to its size. As sample 6 was annealed, the effects of inversion began to appear, until strong inversion clearly became apparent around 8 minutes. Figure 4.7 and 4.8 show C-V curves for 3 and 35 minutes of annealing time. The remaining data can be found in Appendix B. Since the first few measurements of sample 6 did not reach strong inversion, equation 2.28 may not give accurate results. More research needs to be done in this area to determine if the strange behavior of the C-V curves is indeed due to inversion.

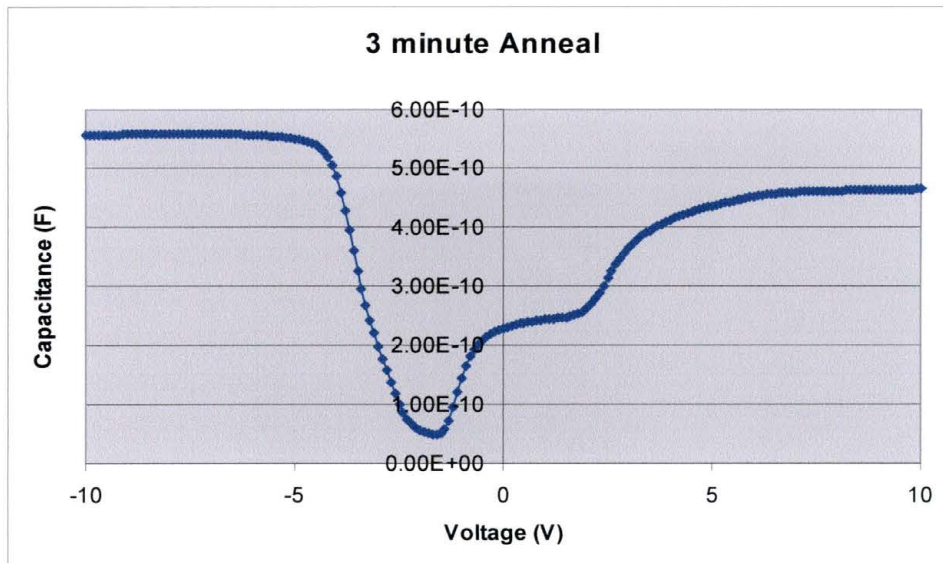


Figure 4.7 C-V Curve of Sample 6, after 3 Minute Anneal

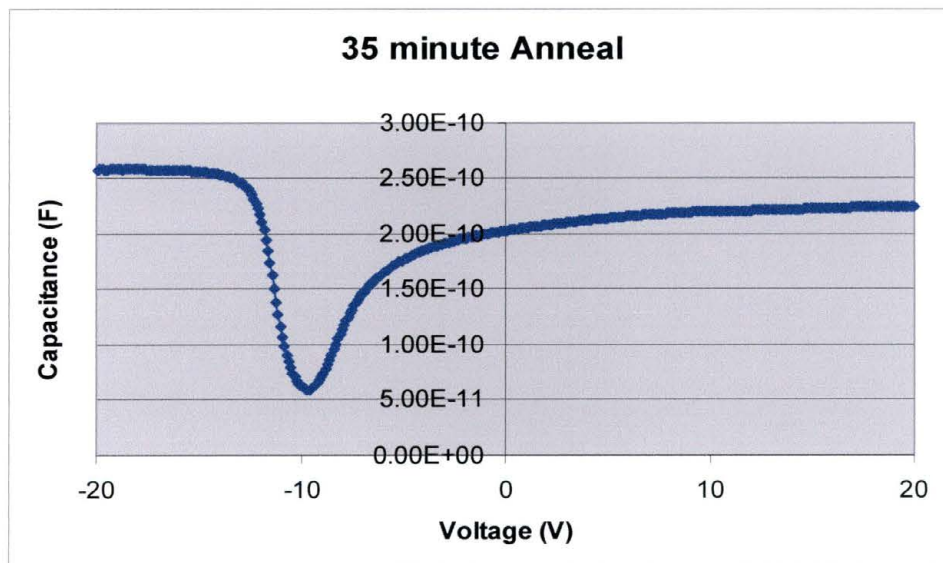


Figure 4.8 C-V Curve of Sample 6, after 35 Minute Anneal

The C-V analysis of sample 6 revealed that the oxide thickness increased from ~27 nm to ~63 nm (Fig. 4.9). The doping concentration was not constant (Fig. 4.10).

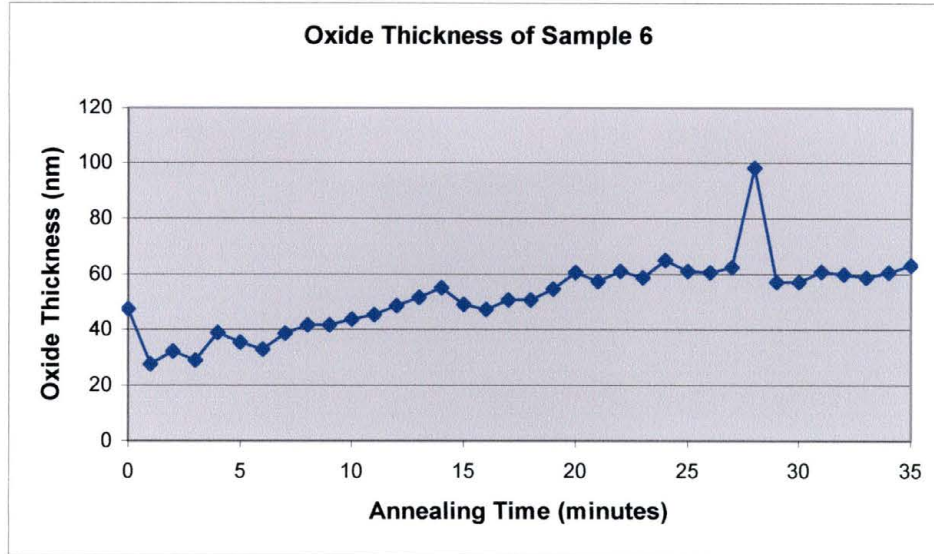


Figure 4.9 Oxide Thickness of Sample 6, Thermally Annealed

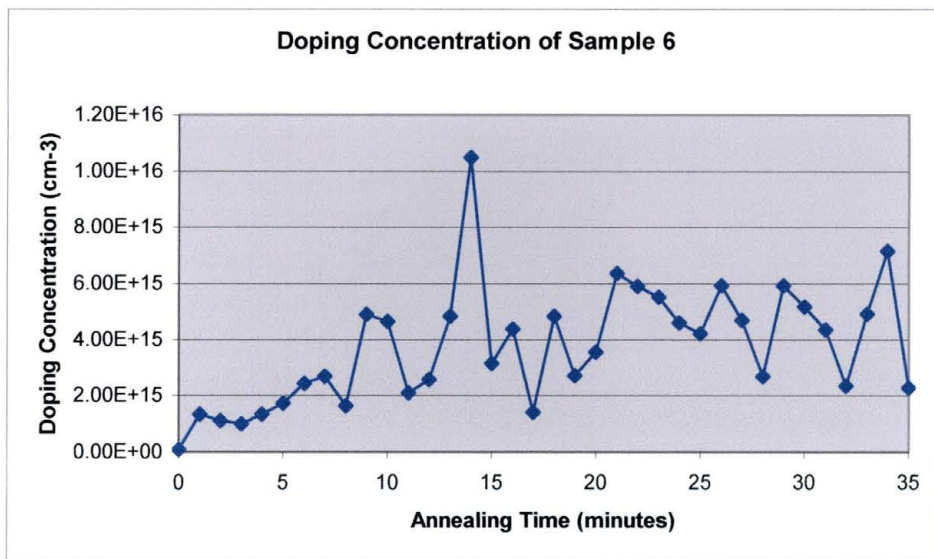


Figure 4.10 Doping Concentration of Sample 6, Thermally Annealed

Since the calculation of oxide thickness using C-V data did not distinguish between different types of oxides, more than one oxide could be present. Combining these results with the ellipsometry results, it is believed that the thickness of the HfO_2 remained constant, while a SiO_2 layer formed and increased in thickness, causing the total oxide thickness to increase.

4.3 Athermally Annealed Samples

4.3.1 FTIR Results

Reflectance spectra of an unannealed sample, a thermally annealed sample, and an athermally annealed sample are shown in figure 4.11. The data for the athermally annealed sample was taken 3 mm from the center of the crater. Analysis of the reflectance spectra was unsuccessful and yielded no results. Further work on this area is needed.

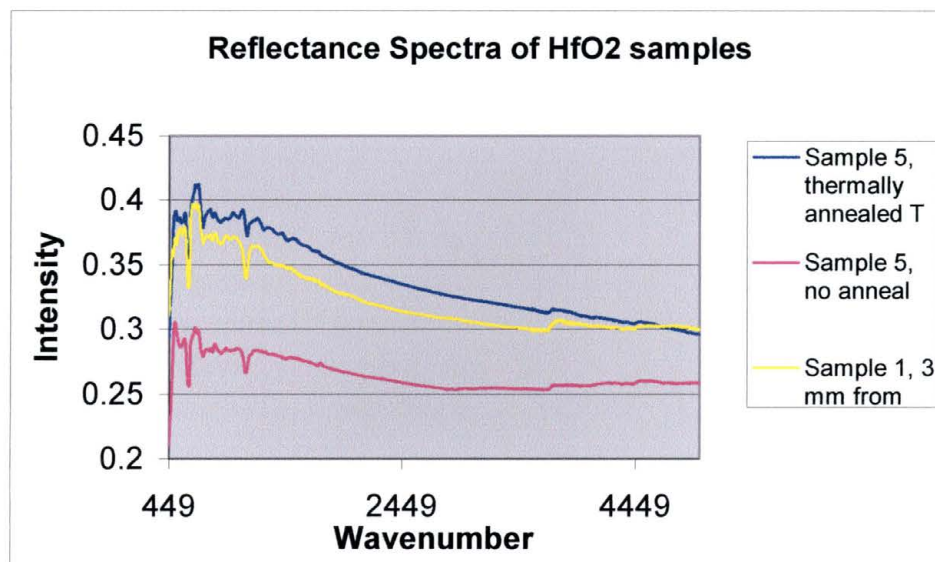


Figure 4.11 Reflectance of HfO₂, Athermally Annealed

Absorbance spectra for sample 1 before and after annealing are shown in figure 4.12. The peak at 1107 cm⁻¹ is the same size for both spectra. Since the area under the peaks did not increase, the amount of oxide present did not change. Therefore, neither the HfO₂ layer nor an interfacial SiO₂ layer could have changed its thickness. The absorbance spectra taken 3 mm and 1.7 cm away from the crater center look the same as the one taken at the crater center (figure 4.13).

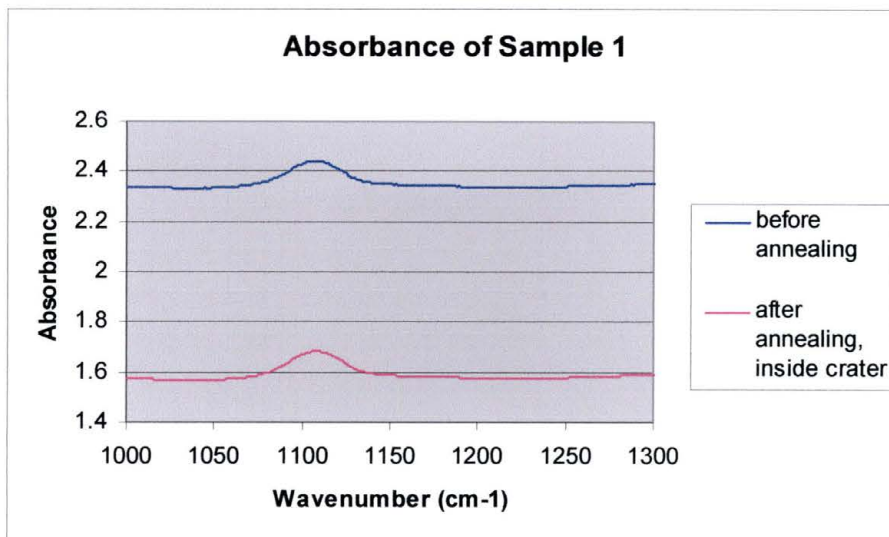


Figure 4.12 Absorbance of Sample 1, Athermally Annealed

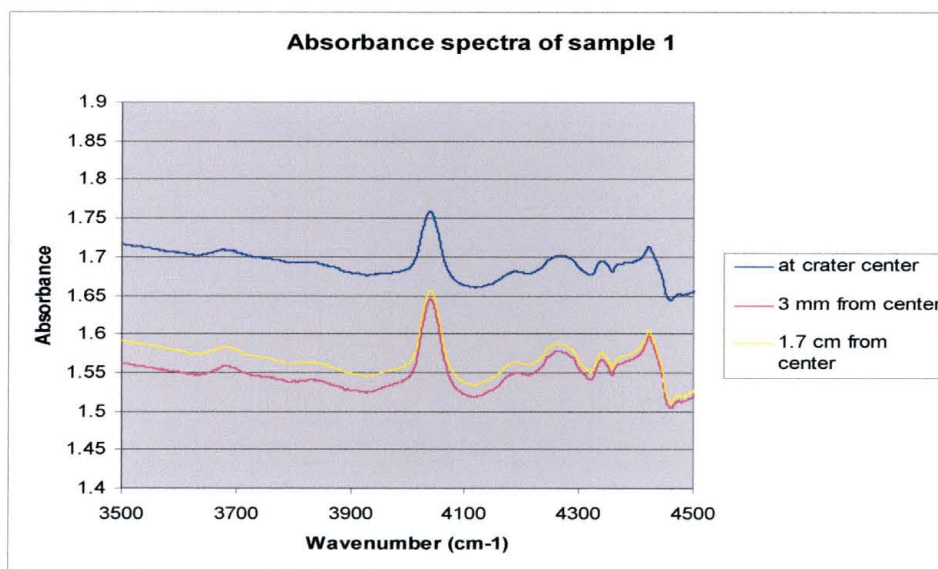


Figure 4.13 Absorbance Spectra of Sample 1, Athermally Annealed

4.3.2 Ellipsometry Results

The index of refraction of the HfO_2 was found to increase. Figure 4.14 shows the values of n and the root mean square error for samples 1, 2, and 3 at distances of 3, 5, 10, 15, and 20 mm from the crater center. The values fluctuate over a distance of 2 cm, but are nearly all slightly larger than the tabulated value for HfO_2 of $n=1.9134$. This suggests

that the laser shock did have an effect upon the oxide layer, but that the effects were not uniform. No SiO₂ layer formed at the interface of samples 1, 2, and 3, and the thickness of the HfO₂ did not change during annealing.

Distance (mm)	Sample 1		Sample 2		Sample 3	
	n	RMSE	n	RMSE	n	RMSE
3	2.0613	0.9623	1.9818	0.4038	2.1782	2.8357
5	2.0055	0.8702	1.9705	0.5099	1.9112	1.7
10	2.0653	0.4808	1.9997	0.5703	1.9769	0.375
15	2.0403	0.2416	2.1157	0.6044	2.0147	0.8675
20	1.9921	0.3832	2.002	1.1642	2.0385	2.6121

Figure 4.14 Index of Refraction of HfO₂ for samples 1,2, and 3

Since the dielectric constant is proportional to n , ϵ_{HfO_2} also increases when the sample is athermally annealed. Using equation 2.1, it can be seen that the equivalent oxide thickness decreases upon athermal annealing.

4.3.3 C-V Analysis Results

Samples 2 and 3 were too small to fit in the mercury probe. C-V analysis of sample 1 after annealing showed that the oxide thickness was 24.3 nm and the carrier concentration is $9.41 \times 10^{13} \text{ cm}^{-2}$. A C-V curve for sample 1 is shown in figure 4.15. It resembles the curve of the unannealed sample 6. The oxide thickness is the same as the unannealed sample, while the carrier concentration increased. These results imply that the charge carriers were activated upon annealing, but no SiO₂ layer formed. However, this curve does not show strong inversion as in figure 4.8. The reason for this is unclear, and more research needs to be performed in this area.

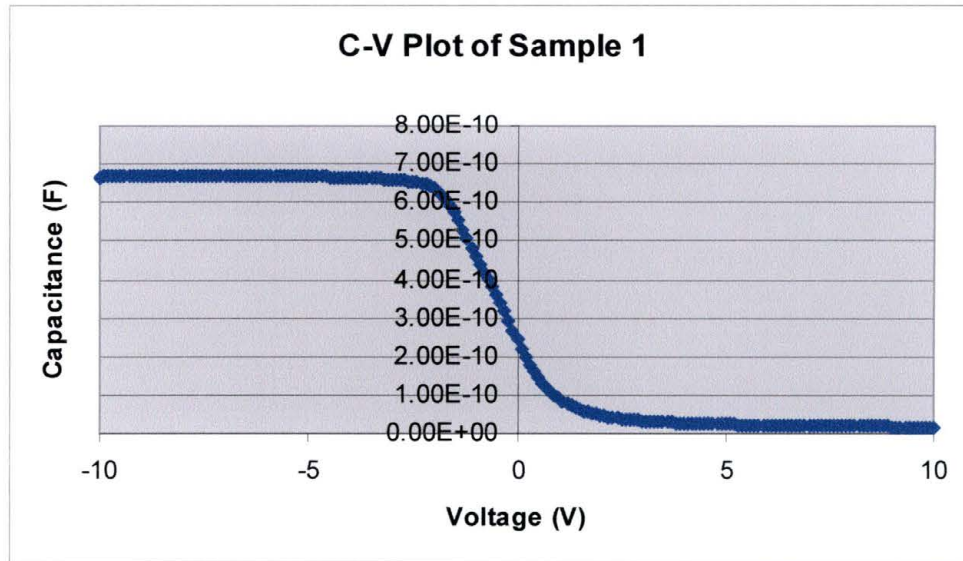


Figure 4.15 C-V Plot of HfO₂, Athermally Annealed

Chapter 5

CONCLUSIONS

The series of measurements performed on thermally and athermally annealed HfO₂ on silicon have revealed important information about changes that occur during both types of annealing. This information can be used to compare the new laser shock technique to the traditional furnace annealing method, and to determine if it is a suitable alternative for annealing substrates with a surface oxide layer.

This research showed that thermal annealing causes silicon in the substrate to diffuse into the oxide, creating a silicon oxide sub-layer. This diffusion is caused by heat. The athermal method involved no heat, and no SiO₂ could be detected, as expected. The athermal method did, however, cause the index of refraction of HfO₂ to increase slightly, while the thermal method produced no such effect.

The exact dielectric constant for any of the materials could not be determined. The method described in chapter 2 using FTIR data has been used by other research groups, but the calculations are too intense for any software available in this lab. Further research would involve a continuation of these calculations. If the dielectric constant could be calculated exactly, the equivalent oxide thickness could be determined from FTIR data alone.

The capacitance-voltage results were interesting and unexpected. The C-V curves seemed to show inversion for the thermally annealed sample, but not for the unannealed

or the athermally annealed sample. More research can be done to explain this phenomenon. The capacitance-voltage analysis provided a result for the oxide thickness. The thickness increased with time as the thermally annealed sample was heated due to formation of an interfacial oxide layer, while it remained the same for the athermally annealed sample.

Further research would include the study of other gate oxides on silicon. Zirconium oxide, ZrO_2 , most resembles hafnium oxide in its optical properties, so it should be studied next.

APPENDIX A

Sample 1 Ellipsometry Data

Distance from Crater Center	Angle of Incidence	Δ	Ψ
3mm	50.0679	159.5	30.45
3mm	69.7988	106.3	16.1
5mm	50.0679	162.1	31.7
5mm	69.7988	107.4	15.75
10mm	50.0679	161.5	30.55
10mm	69.8377	107.5	15.75
15mm	50.0665	161.8	30.9
15mm	69.8767	108.7	15.45
20mm	49.8196	161.7	30.9
20mm	69.9369	108.5	15.95
30mm	49.8196	160.3	31.55
30mm	69.8583	108.2	16.35

Sample 2 Ellipsometry Data

Distance from Crater Center	Angle of Incidence	Δ	Ψ
3mm	50.4896	161.4	30.75
3mm	70.0783	107.3	15.85
5mm	50.5491	161.3	31
5mm	70.0783	107.2	15.8
10mm	50.5491	161.9	30.8
10mm	69.8902	107.4	15.95
15mm	50.0665	161.6	30.6
15mm	69.749	106.7	15.5
20mm	50.5518	160.4	30.8
20mm	69.9369	104.4	16.5

Sample 3 Ellipsometry Data

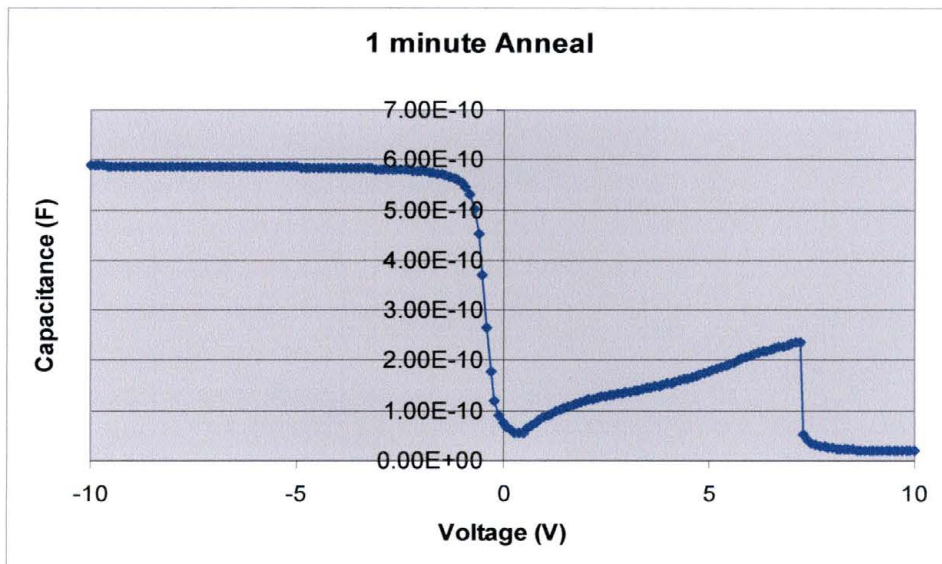
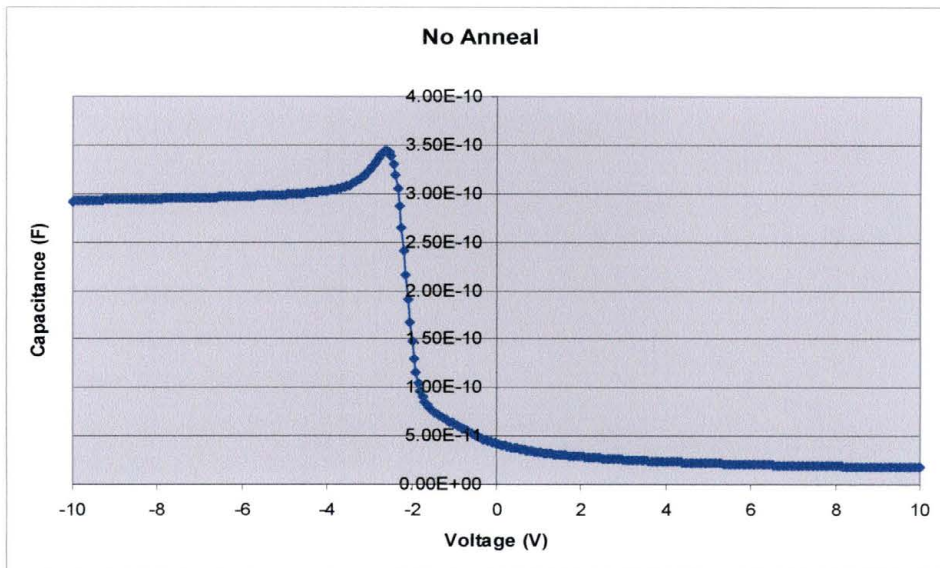
Distance from Crater Center	Angle of Incidence	Δ	Ψ
3mm	49.9442	162.6	26.95
3mm	69.8902	103.7	16.85
5mm	49.9442	163.4	32.5
5mm	69.9369	104.8	17.05
10mm	49.7551	161.8	30.6
10mm	69.9369	110.5	15.7
15mm	49.9346	161.5	30.95
15mm	69.749	106.9	16.35
20mm	50.5518	158.9	31.1
20mm	68.7012	102.5	17.45

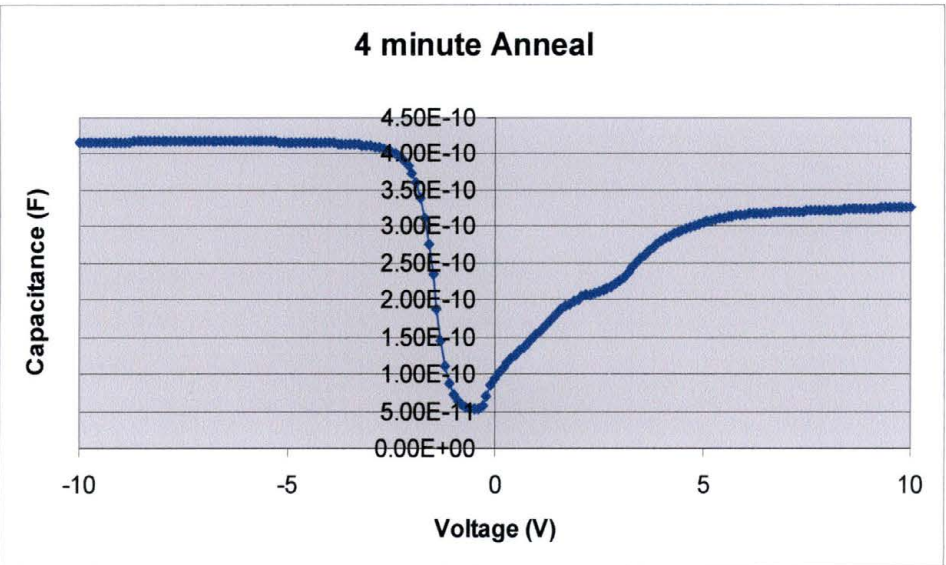
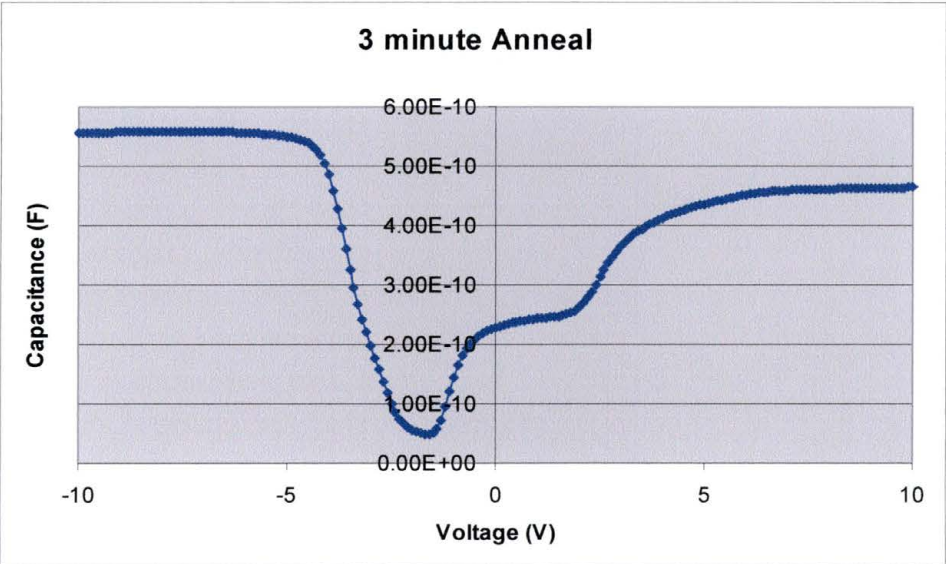
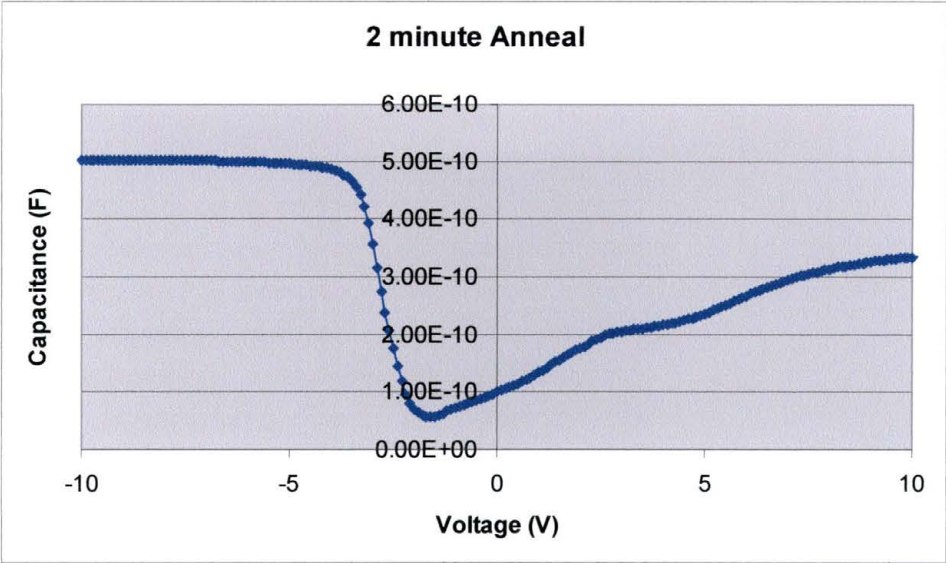
Sample 6 Ellipsometry Data

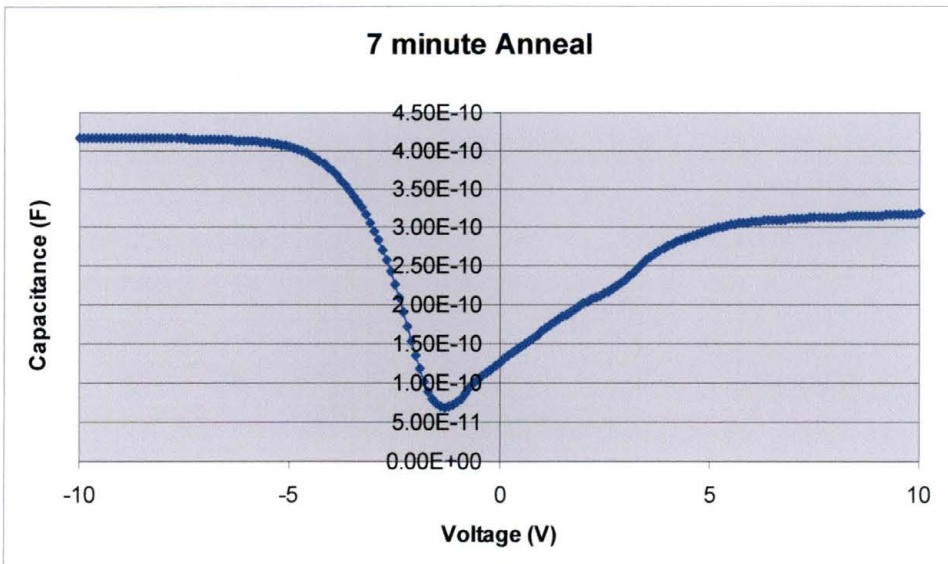
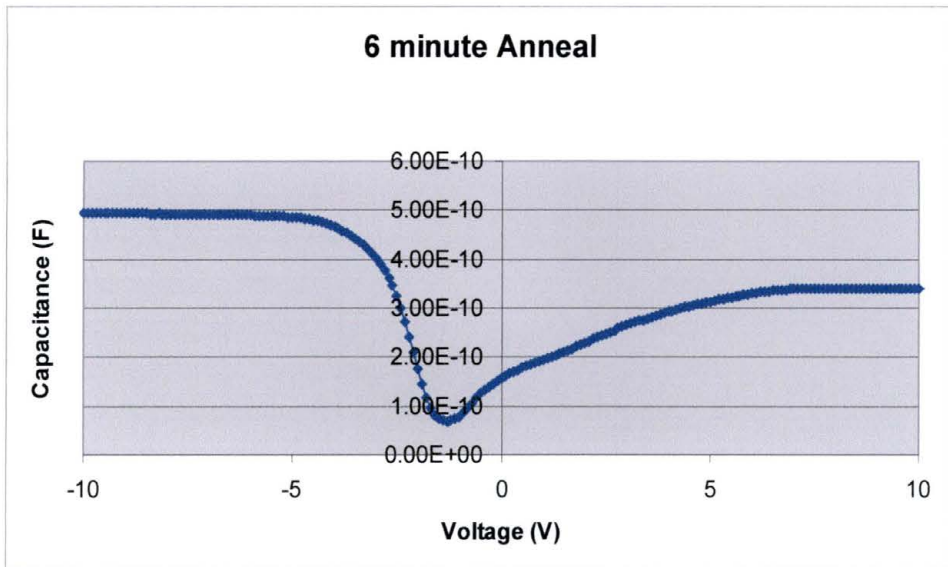
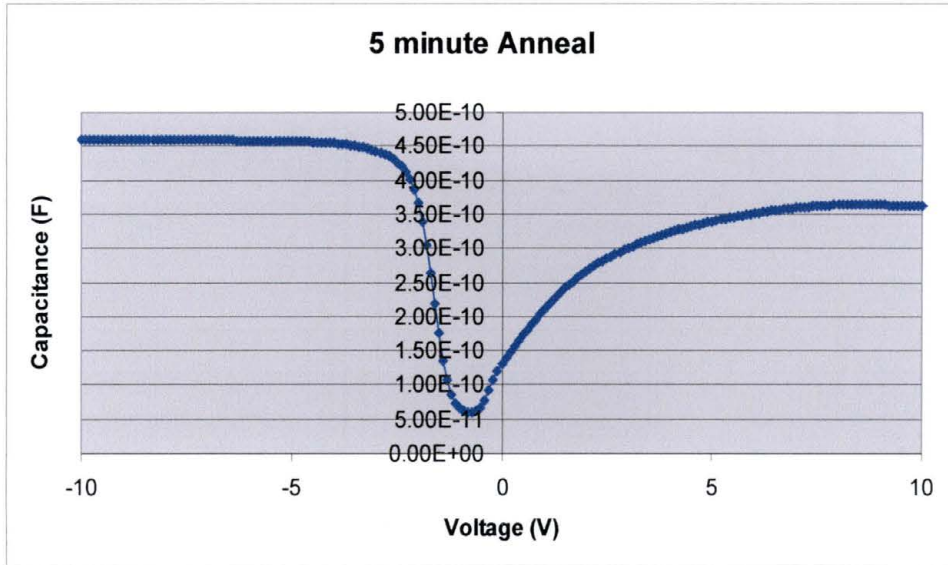
Minutes Annealed	Angle of Incidence	Δ	Ψ
0	49.9378	163.5	31.45
0	69.6654	112.5	15.3
1	49.6903	160	30.65
1	68.0292	106.5	16.15
2	49.5159	157.5	30.7
2	69.6755	99.3	17.75
3	49.5159	166.6	30.55
3	69.8663	96.8	18.2
4	49.6436	155.8	30.3
4	69.8743	94.2	18.75
5	49.8178	153.4	30.75
5	69.7533	90.9	19.75
6	49.816	152.3	30.9
6	69.7533	88.7	20.5
7	49.816	151	30.9
7	69.8623	87.2	21.55
8	49.816	148.9	30.9
8	69.8623	83.6	22.9
9	49.816	148.8	31.3
9	69.7844	84	22.4
10	50.2487	146.6	31.25
10	69.7844	81.4	24.05
11	50.2487	144.7	31.6
11	69.9589	80.2	24.3
12	50.0016	143.9	32
12	69.9589	79	24.8
13	50.0016	144.8	31.95
13	69.8605	80	25.1
14	50.3644	142.5	32.5
14	69.8605	77.5	26.45
15	50.3644	140.4	32.65
15	69.7988	76.1	26.8
16	50.2442	139.9	33.2
16	69.7988	75.2	27.65
17	50.2442	140.8	33.4
17	69.8173	75.7	28.25

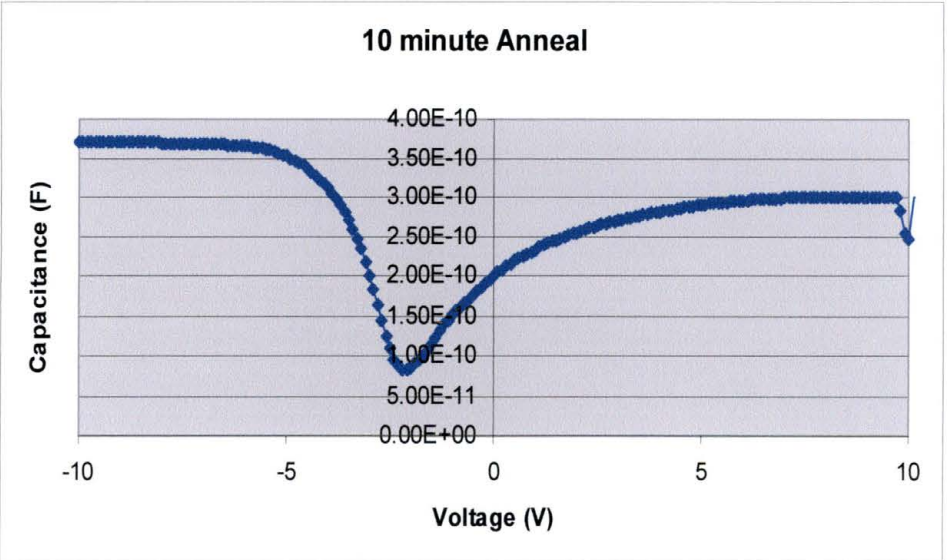
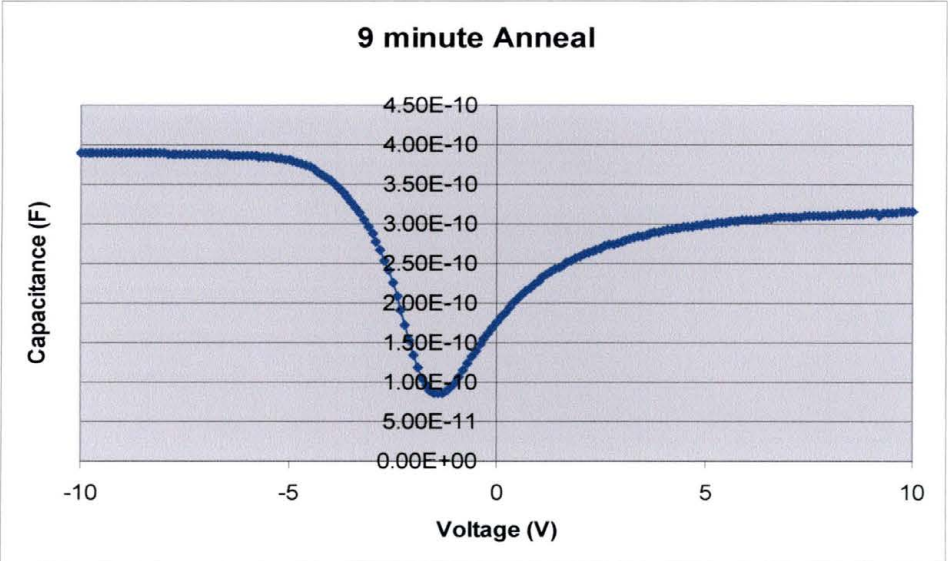
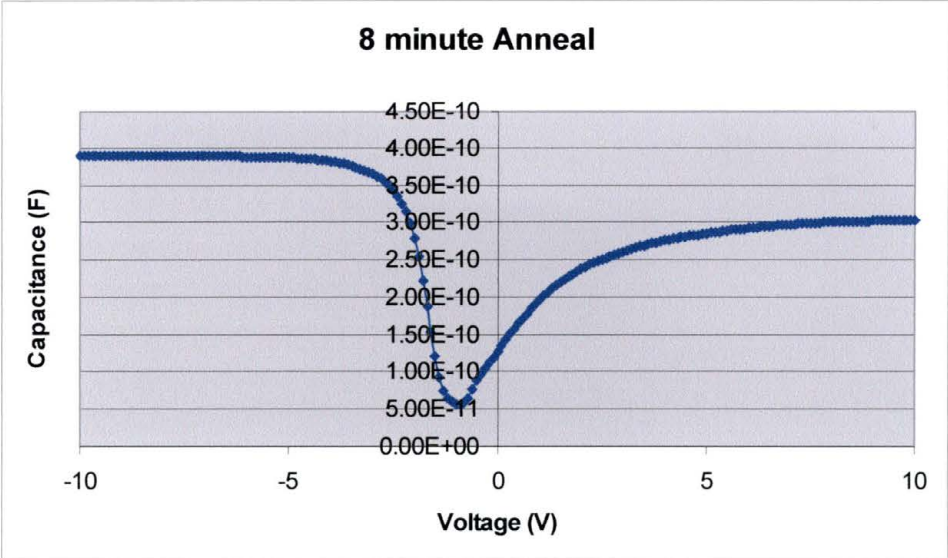
Minutes Annealed	Angle of Incidence	Δ	Ψ
18	49.941	138.7	33.6
18	69.8173	74.8	28.35
19	49.941	136.8	34.4
19	69.8966	73.1	30
20	49.9394	135.7	35
20	69.8966	72	30.6
21	49.9394	135.8	35.15
21	69.7988	72.7	30.55
22	50.4896	133.9	36.1
22	69.8377	71.7	31.5
23	49.9442	134.7	35.4
23	69.8767	71.5	30.65
24	49.9346	133	36.9
24	69.8783	70	32.35
25	49.6923	133.5	38.5
25	69.7737	70.8	33.8
26	49.6923	132.8	38.6
26	70.028	69.8	34.9
27	49.3158	130.3	42.45
27	69.807	67	36.15
28	49.816	131.9	41.4
28	69.807	68.2	36.75
29	49.816	130.6	42.95
29	69.7175	66.7	37.7
30	49.6333	133.7	44.55
30	69.7175	65.8	40.95
31	49.6333	128.1	47.25
31	70.0385	65.3	40.75
32	49.5681	129.9	45.95
32	70.0385	66.7	40.65
33	49.5681	129.3	48.05
33	69.9005	65.4	41.8
34	50.1243	142.4	44.9
34	69.9005	64.2	42.5
35	50.1243	132.7	51.3
35	69.809	64.4	44.25

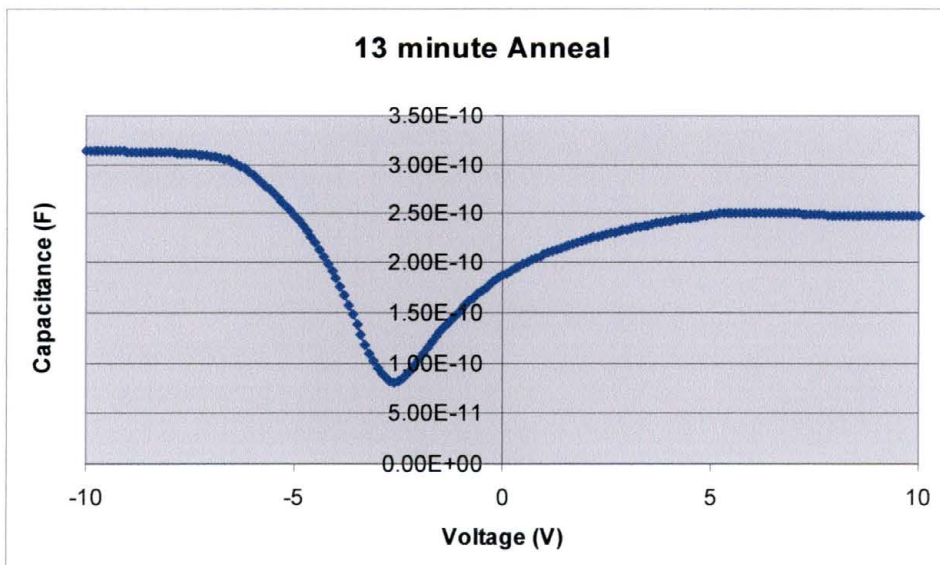
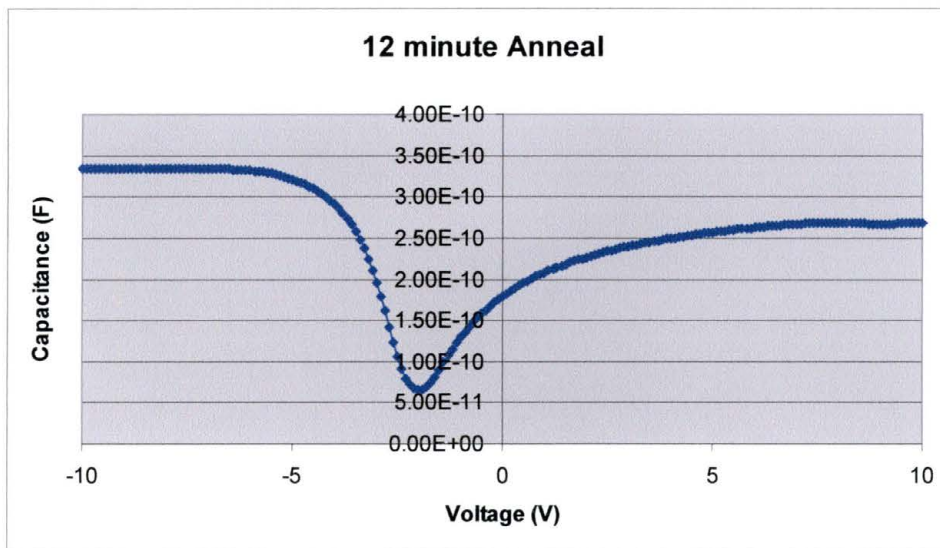
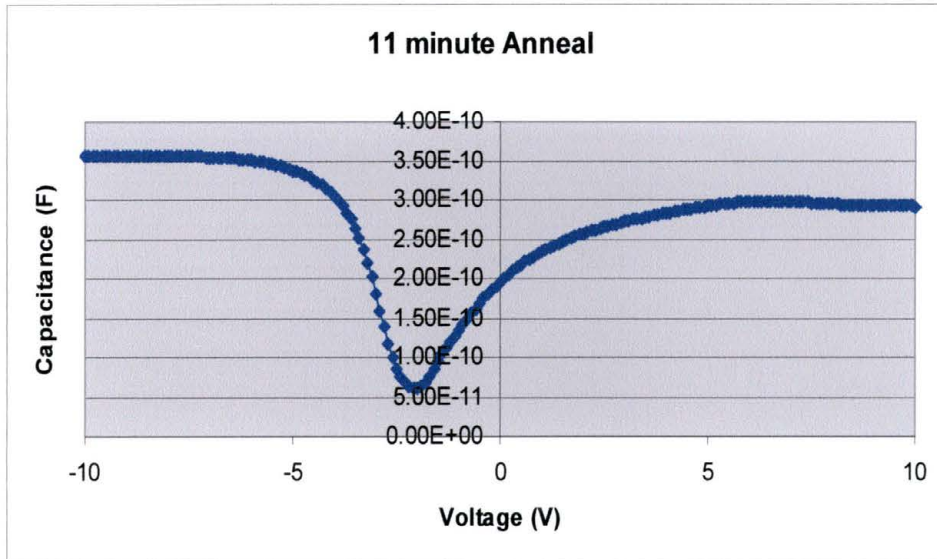
APPENDIX B

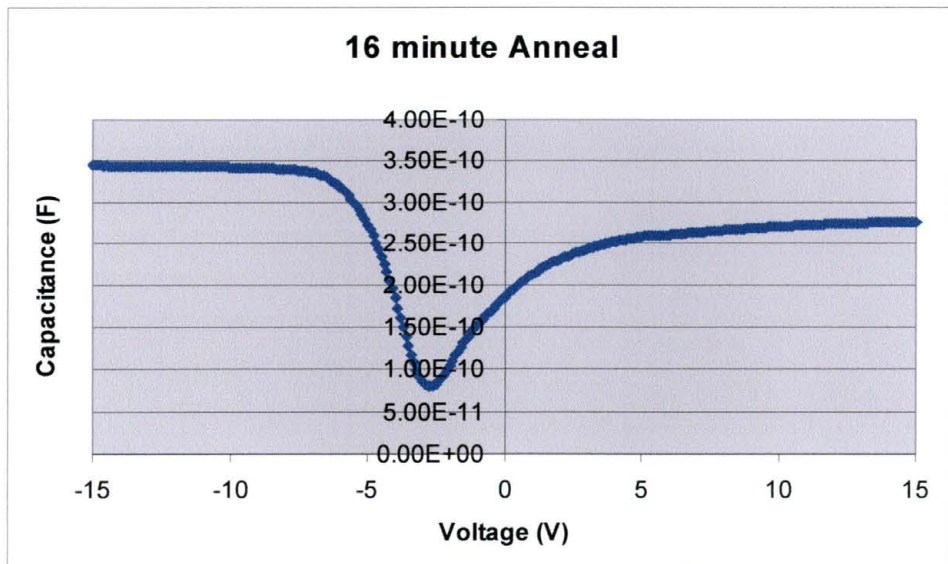
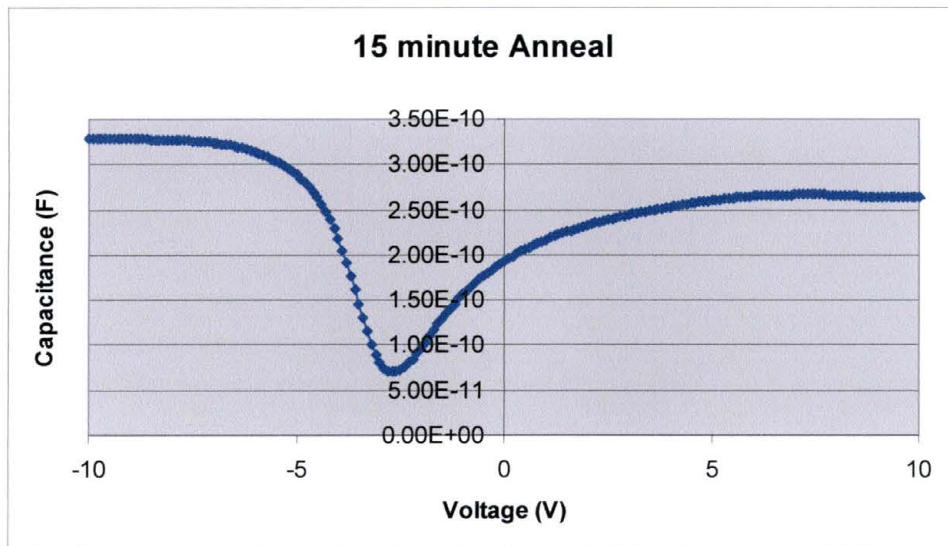
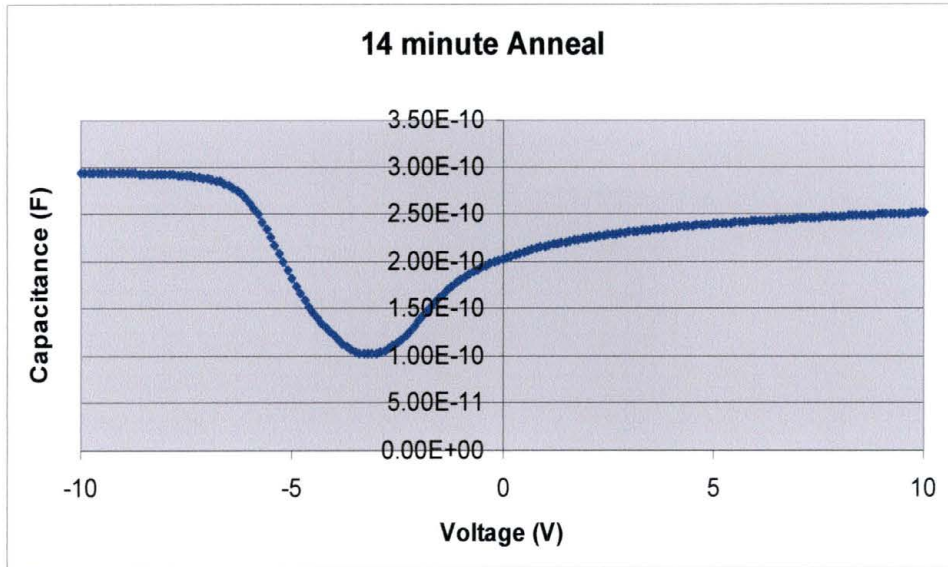


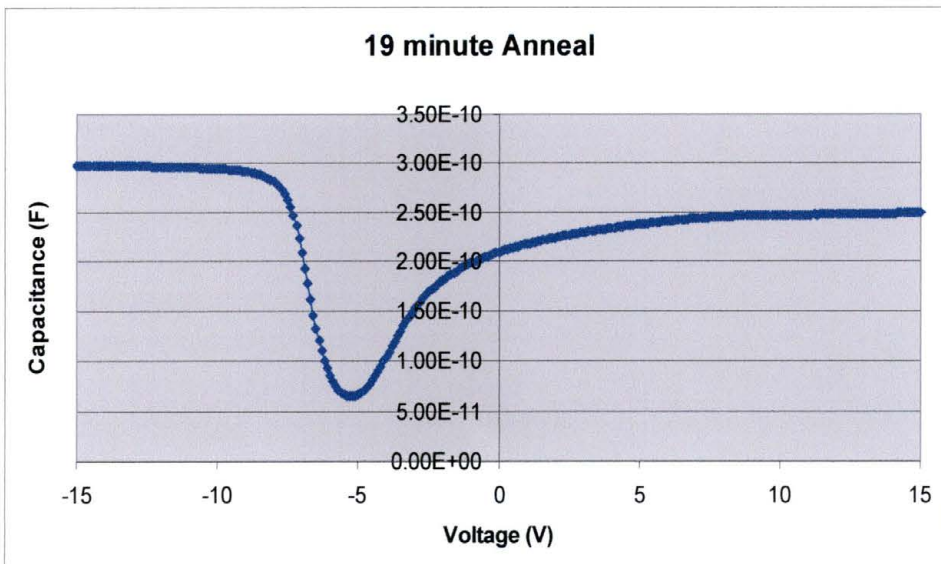
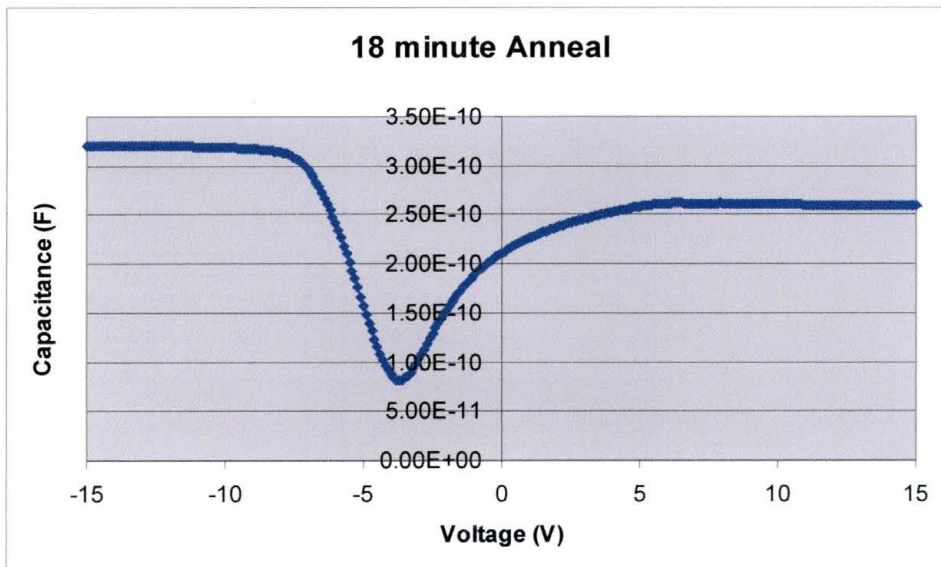
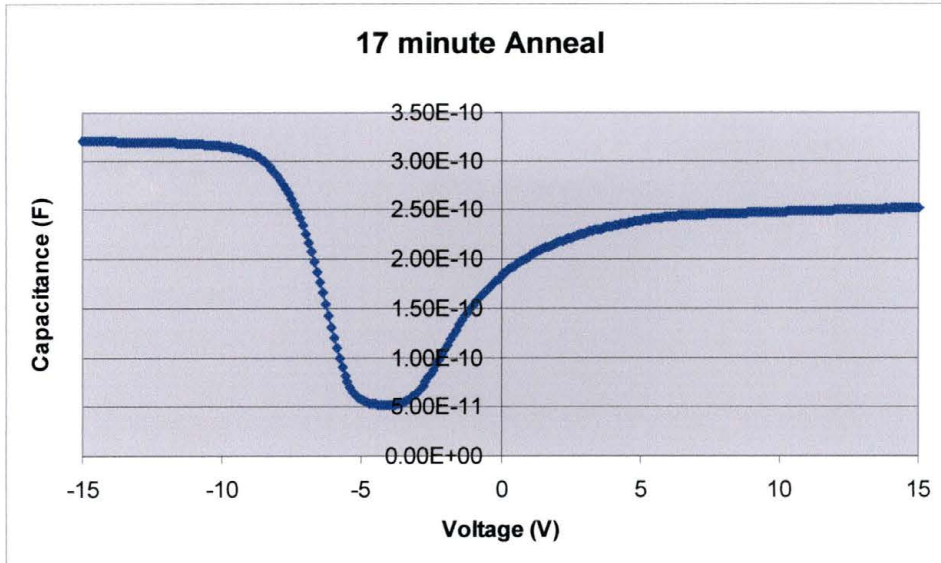


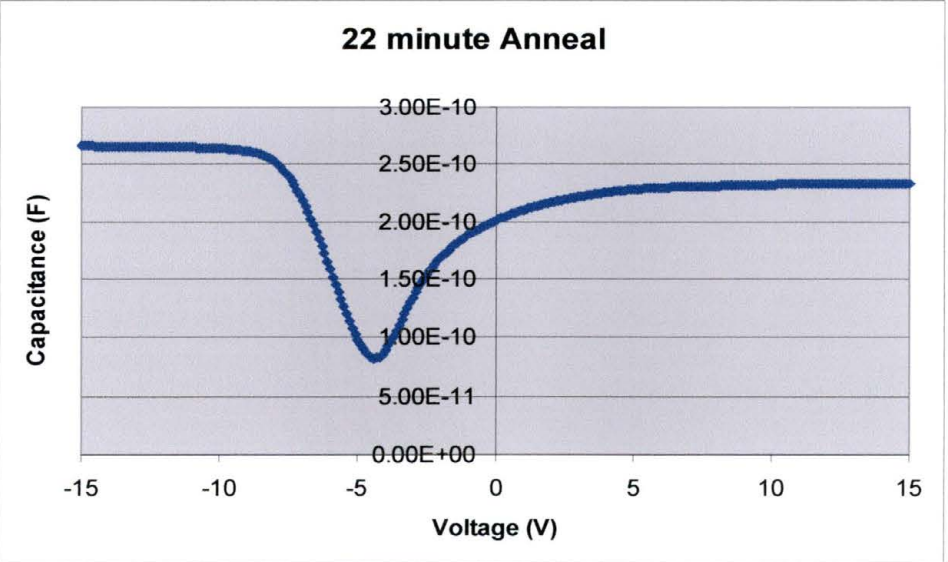
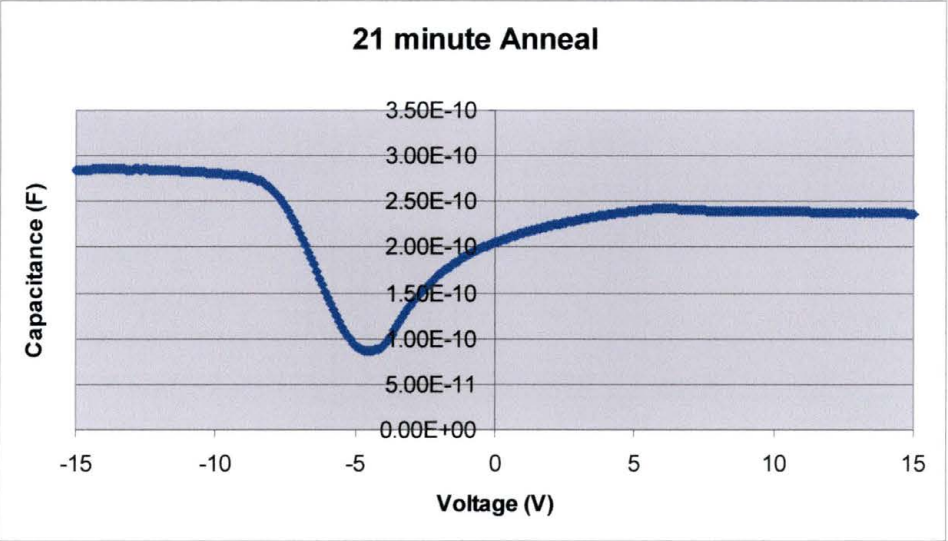
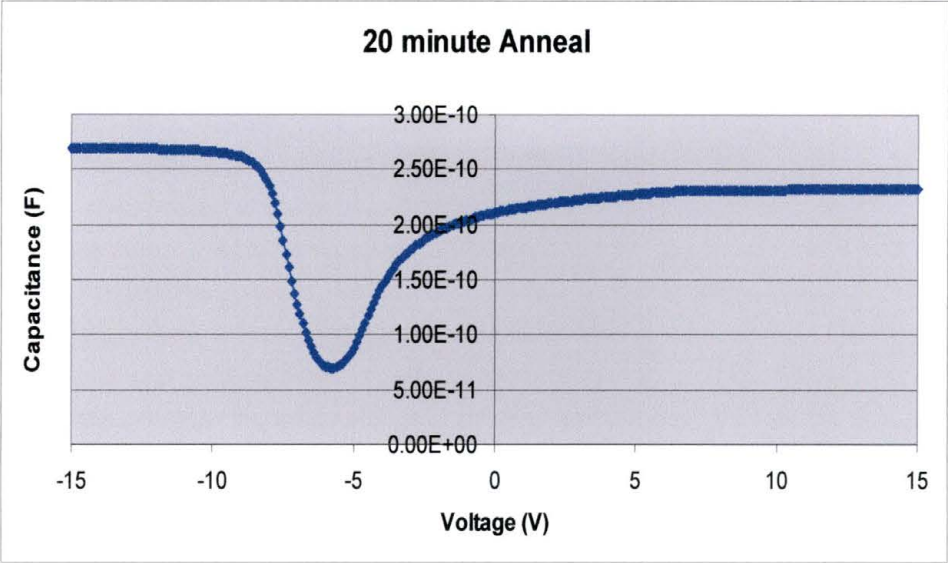


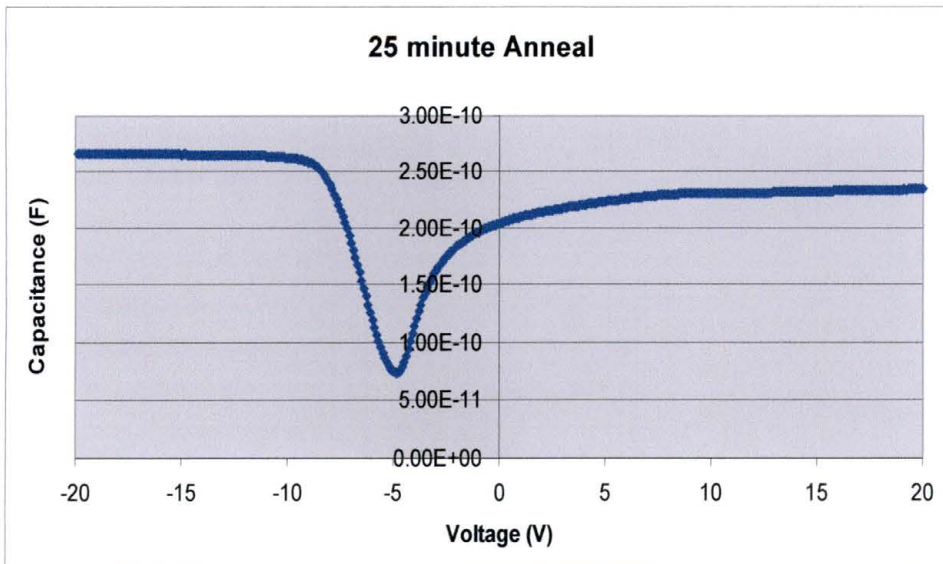
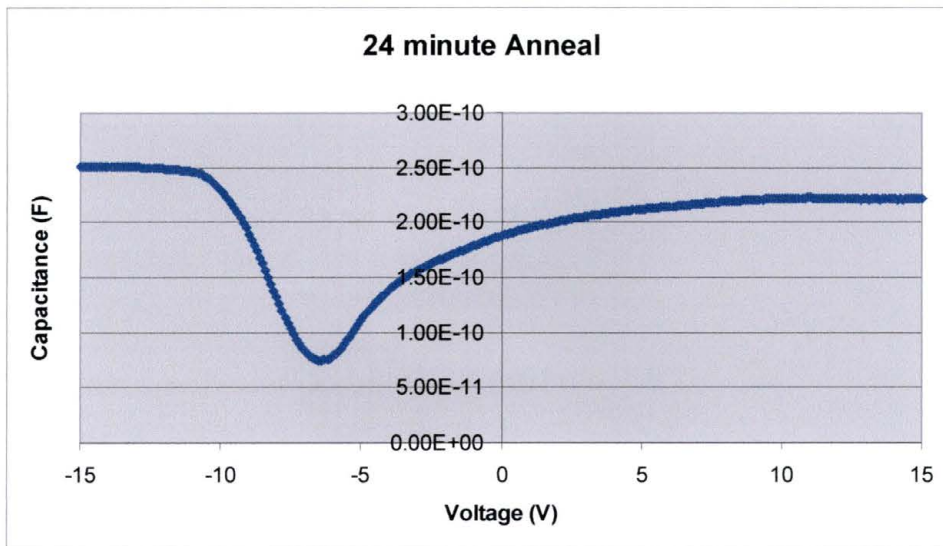
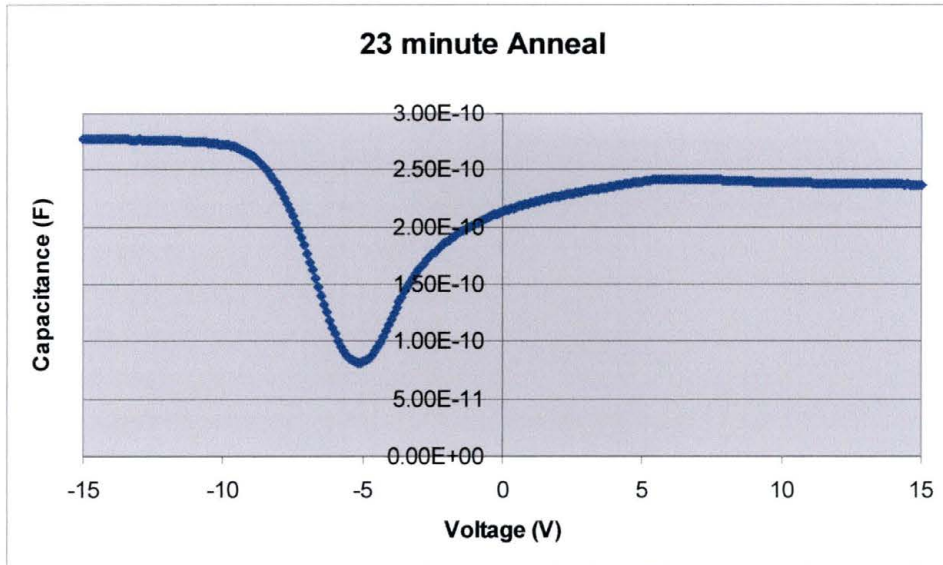


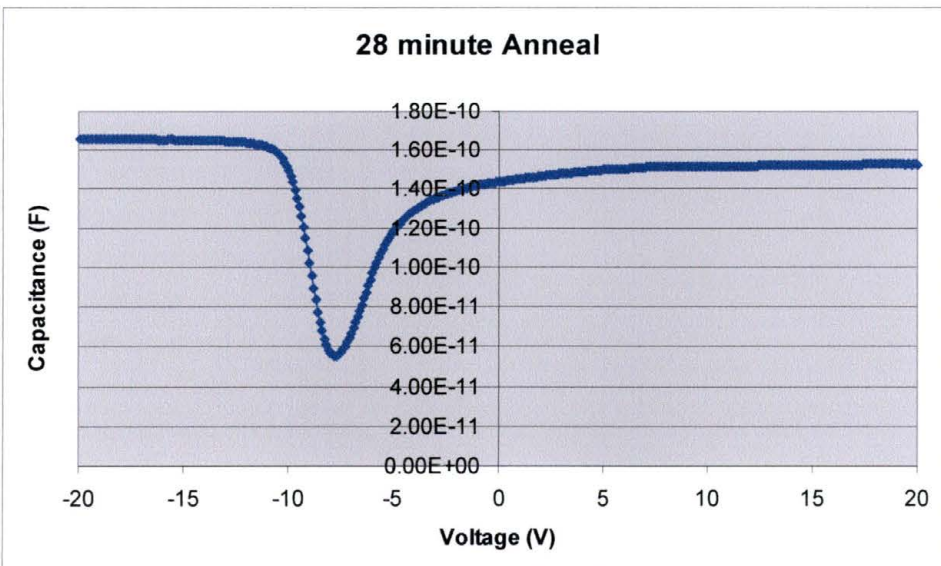
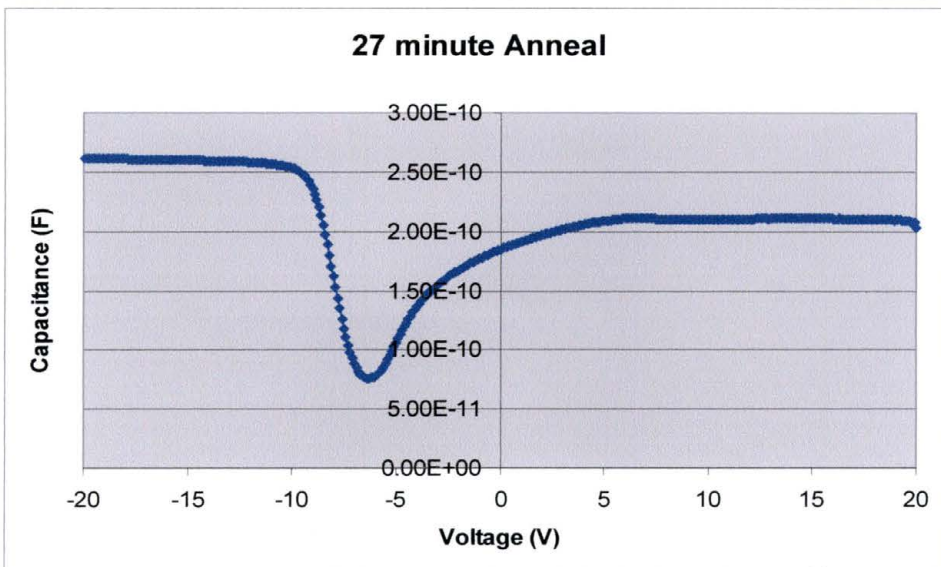
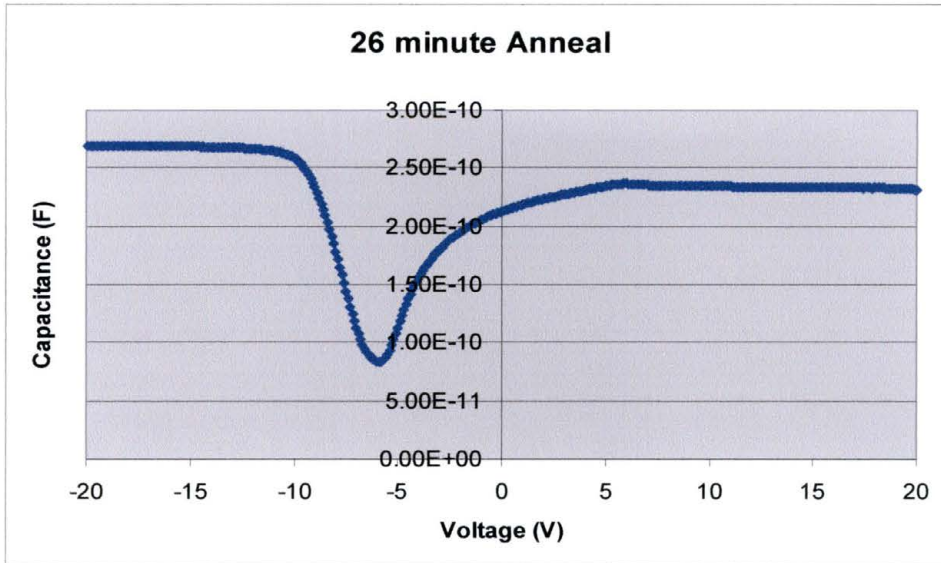


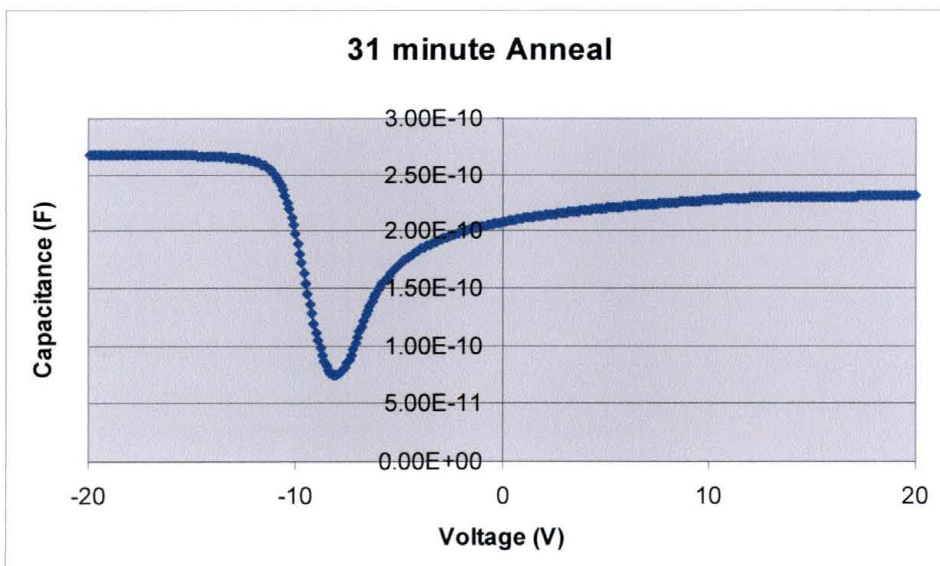
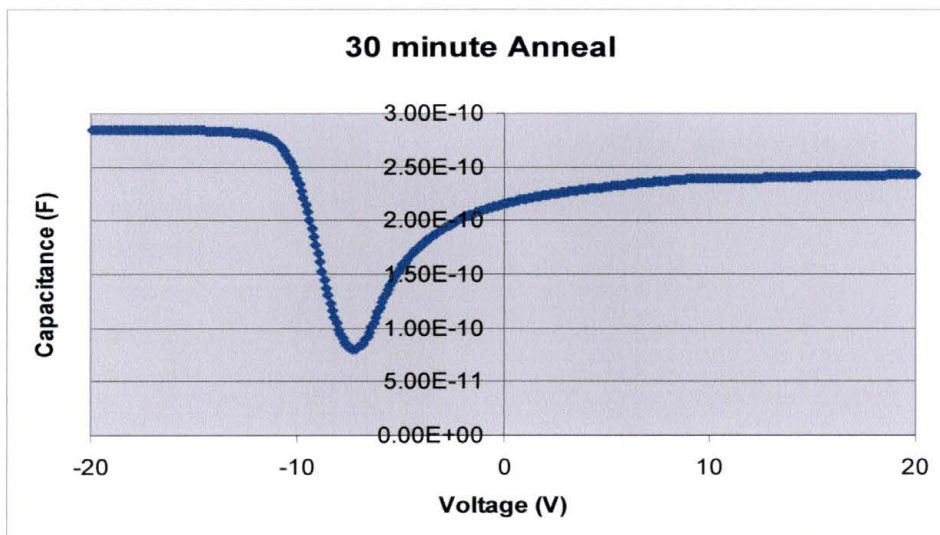
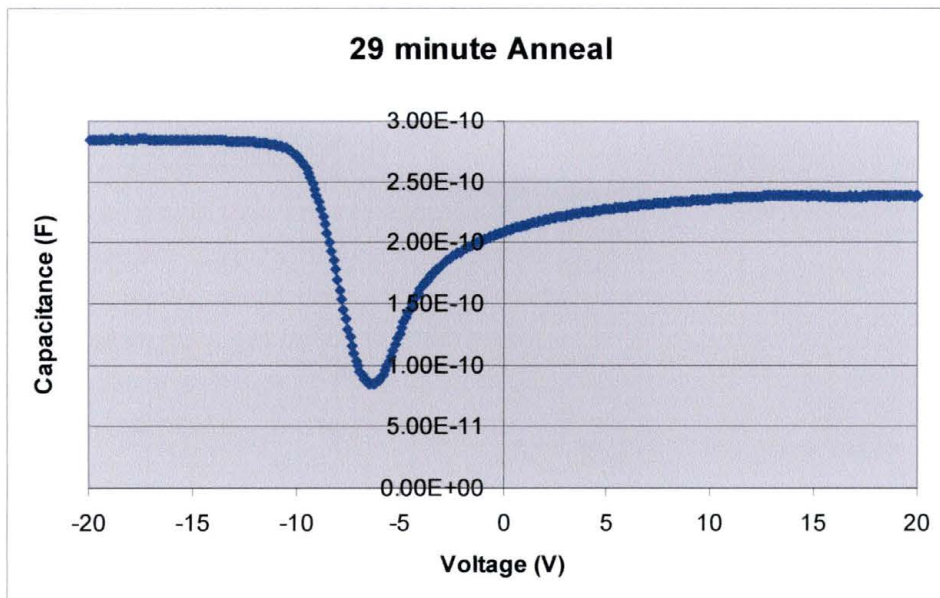


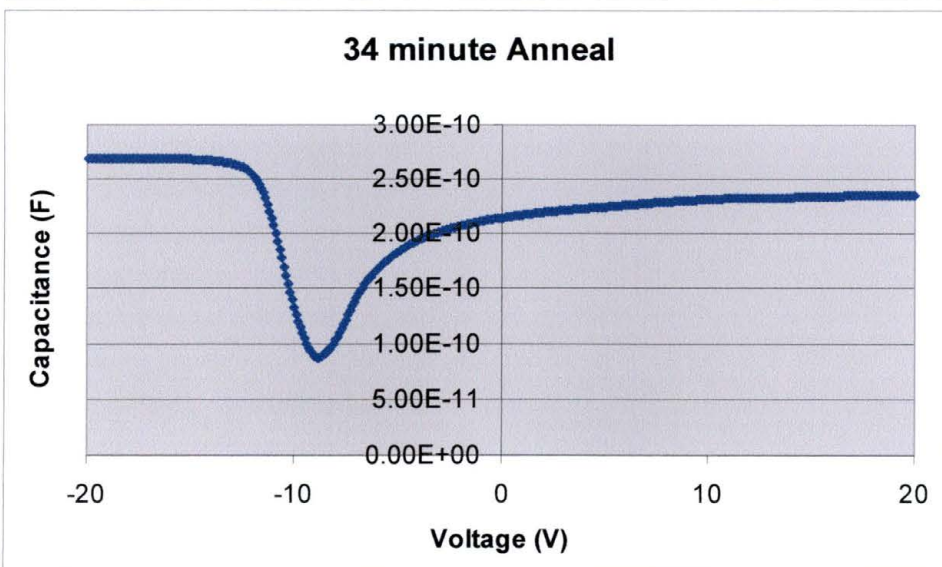
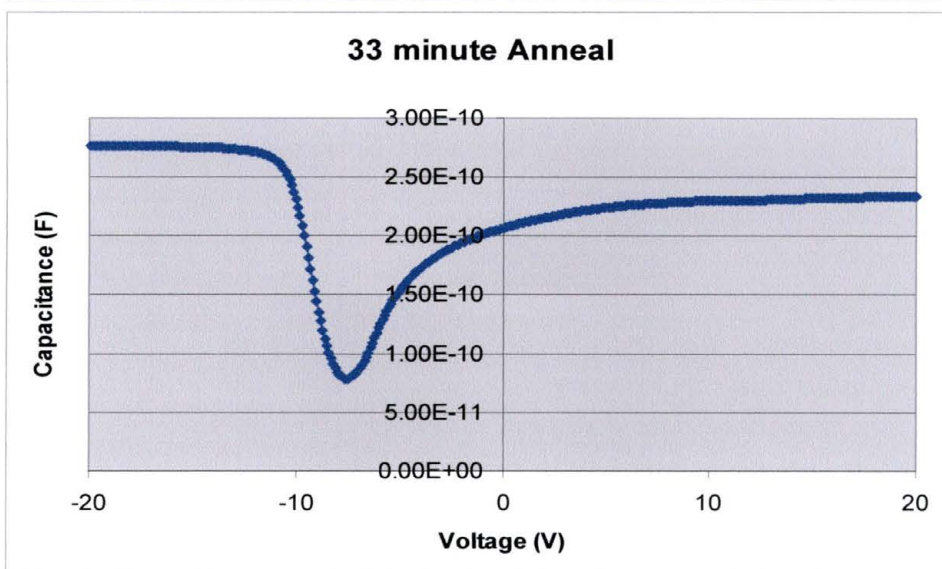
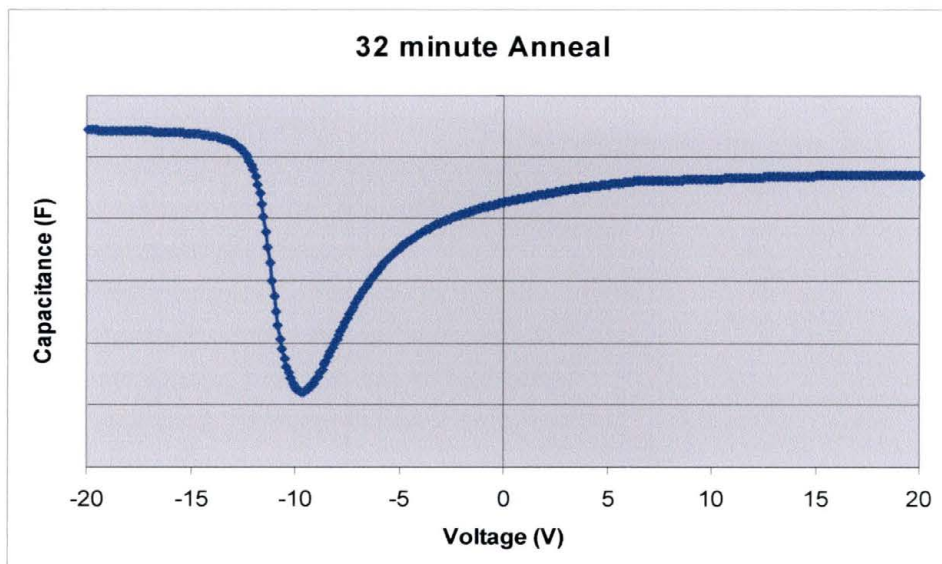


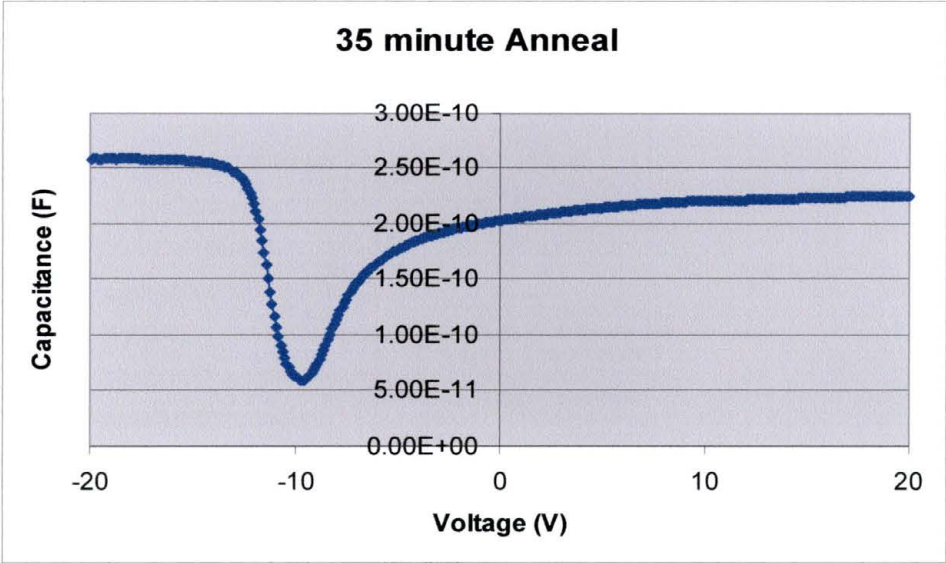












REFERENCES

- ¹W. Arden, J. Bruines, G. Goltz, F. Roosmalen, T. Fukushima, S. Kawamura, T. Masuhara, M. Yoshimi, A. Chung, J. Moon, H. Yoon, K. Chiu, C. Hu, G. Hu, D. Lee, C. Lu, C. Wang, P. Yang, B. Doering, P. Gargini, and J. Matisoo, *International Technology Roadmap to Semiconductors*, 2002 Update.
- ²G. D. Wilk and R. M. Wallace, *Appl. Phys. Lett.* **74**, 2854 (1999).
- ³J. Lee and B. Lai, in *Handbook of Thin Film Materials*, edited by H. Nalwa (Academic, New York, 2002), Vol. 3, p. 1.
- ⁴D. Donnelly, B. Covington, J. Grun, R. Fischer, M. Peckerar, and C. Felix, *Appl. Phys. Lett.* **78**, 2000 (2001).
- ⁵S. M. Sze, *Physics of Semiconductor Devices* (Wiley, New York, 1981).
- ⁶R. C. Jaeger, *Introduction to Microelectronic Fabrication* (Addison Wesley Publishing Company, New York, 1993).
- ⁷<http://hyperphysics.phy-astr.gsu.edu/hbase/hframe.html>
- ⁸J. Grun, C. Manka, C. Hoffman, J. Meyer, O. Glembocki, S. Kaplan, S. Qadri, E. Skelton, D. Donnelly, and B. Covington, *Phy. Rev. Lett.* **78**, 1584 (1997).
- ⁹R. Bell, *Introductory Fourier Transform Spectroscopy* (Academic Press, New York, 1972).
- ¹⁰S. Davis, M. Abrams, and J. Brault, *Fourier Transform Spectroscopy* (Academic Press, San Diego, 2001).
- ¹¹O. Heavens, *Optical Properties of Thin Solid Films* (Dover Publications, New York, 1991).
- ¹²A. Fontcuberta i Morral, J. Zahler, H. Atwater, M. Frank, Y. Chabal, P. Ahrenkiel, and M. Wanlass, *Proceedings of the Material Research Society, MRS*, San Francisco, CA, 2003.
- ¹³H. G. Tompkins and W. A. McGahan, *Spectroscopic Ellipsometry and Reflectometry* (Wiley, New York, 1999).
- ¹⁴W. Geerts, *Manual for mercury probe*

¹⁵D. K. Schroder, *Semiconductor Material and Device Characterization* (Wiley, New York, 1990).

¹⁶T. Hori, *Gate Dielectrics and MOS ULSIs* (Springer, New York, 1997).

VITA

Heather Marie (Cain) Verdeck was born on July 30, 1979 in Virginia Beach, Virginia, to Susan Lee Cain and Albert Bryan Cain. After finishing her preliminary studies at Princess Anne High School in Virginia Beach, she moved to Texas and enrolled in Southwest Texas State University. She received a Bachelor of Science degree in physics from Southwest Texas State University in May 2001. During her undergraduate career, she served as an intern at NASA Langley in Hampton, Virginia, and at International Sematech in Austin, Texas. She returned to Southwest Texas State University (now Texas State University) in August 2002 to begin work on her Master of Science degree.

Permanent Address: 3609 Kim Terrace
 Virginia Beach, VA 23452

This thesis was typed by Heather Marie Cain.